Neuroscience Research 77 (2013) 110–119

Contents lists available at ScienceDirect

Neuroscience Research

journal homepage: www.elsevier.com/locate/neures

Activation of extracellular signal-regulated kinase in the trigeminal ganglion following both treatment of the dura mater with capsaicin and cortical spreading depression

Tatsuo Iwashita*, Toshihiko Shimizu, Mamoru Shibata, Haruki Toriumi, Taeko Ebine, Megumi Funakubo, Norihiro Suzuki

Department of Neurology, School of Medicine, Keio University, Japan

ARTICLE INFO

Article history:
Received 19 June 2013
Received in revised form 5 August 2013
Accepted 7 August 2013
Available online 17 August 2013

Keywords:
ERK
Trigeminal ganglion
TRPV1
Cortical spreading depression

ABSTRACT

Extracellular signal-regulated kinase (ERK) is known to be phosphorylated after exposure to noxious stimuli. In this study, we investigated the response in the dura mater to nociceptive stimulation, which is thought to be responsible for the pathogenesis of headaches, including migraines. We also examined the level of ERK phosphorylation in the trigeminal ganglion following cortical spreading depression (CSD), which is thought to play an important role in migraine pathophysiology. Western blot and immunohistochemical analyses showed a significant increase in the ERK phosphorylation levels 3 min following an application of 10 mM capsaicin to the dura mater. This increase was inhibited after an application of the TRPV1 antagonist capsazepine or a MEK inhibitor. An immunohistochemical analysis revealed that most of the small-sized trigeminal ganglion neurons with TRPV1-immunoreactivity that innervate the dura mater exhibited pERK-immunoreactivity, suggesting that these neurons had responded to nociceptive stimulation. CSD increased the level of ERK phosphorylation 30 min after its elicitation, and this response was inhibited by a prior intraventricular administration of TRPV1 antagonist. These results indicate that CSD can activate dural TRPV1 to send nociceptive signals to the trigeminal system, and they provide important clues regarding the relationship between CSD and the trigeminovascular system.

1. Introduction

Extracellular signal-regulated protein kinases (ERKs) are mitogen-activated protein kinases (MAPKs) that are activated by membrane depolarization and calcium influx. ERK activation is also regulated by upstream kinases, which are referred to as MAPK/ERK kinases (Roux and Blenis, 2004). The phosphorylation of ERK in response to the noxious stimulation of peripheral transient receptor potential vanilloid subfamily member 1 (TRPV1) receptors has been observed in the dorsal root ganglia, spinal dorsal horn, and the trigeminal caudal nucleus (Ji et al., 1999; Dai et al., 2002; Shimizu et al., 2006). Accordingly, changes in ERK phosphorylation levels can be regarded as a sensitive marker for TRPV1 stimulation. The phosphorylated ERK is known to induce post-translational and transcriptional regulation, and these changes are likely related to the generation of nociceptive-specific pain plasticity and to inflammation-induced pain hypersensitivity (Obata and Noguchi, 2004; Ji et al., 2009). Recent animal experiments revealed the changes in ERK phosphorylation levels in the trigeminal ganglion and meningeal arteries following the nociceptive stimulation of the dura mater, and these results are considered to contribute to the migraine-related sensitization (Yan et al., 2012; Zhang et al., 2013).

The dura mater is widely recognized as one of the most important structures in the generation of headaches (Olesen et al., 2009). It is densely innervated by trigeminal nerve fibers that contain calcitonin gene-related peptide and substance P (Andres et al., 1987; Uddman et al., 1989; Reuss et al., 1992; Messlinger et al., 1993). In addition to these nerve fibers, we have demonstrated the existence nerve fibers in the dura mater that are positive for the TRPV1 receptor, which is known to be a capsaicin-, proton- and heat-sensitive, cation-selective channel. We have also reported that these TRPV1-containing nerve fibers are derived from the trigeminal ganglion (Shimizu et al., 2007).

In addition to the dura mater, cortical spreading depression (CSD) is responsible for the development of migraine aura (Olesen et al., 1990). CSD was initially reported by Leão in the rabbit cerebral cortex as a reversible response that manifested itself through the depolarization of neurons and glial cells that was followed by the sustained suppression of spontaneous neuronal activity (Leão, 1944). CSD is known to be provoked by chemical stimulation by

* Corresponding author at: Department of Neurology, School of Medicine, Keio University, 35 Shinanomachi, Shinjuku-ku, Tokyo 160-8582, Japan.
Tel.: +81 3 5363 3788; fax: +81 3 3353 1272.
E-mail address: iwashita@a6.keio.jp (T. Iwashita).

0168-0102/$ – see front matter
http://dx.doi.org/10.1016/j.neures.2013.08.001

potassium and to spread through the cortical tissue from the initiation site at a rate of 2–5 mm/min, suppressing the EEG and deflecting direct current (DC) potential. Hadjikhani et al. observed blood oxygenation level-dependent signal changes during visual aura in migraine patients and suggested the possibility that CSD generates the aura in the human visual cortex (Hadjikhani et al., 2001). However, the relationship between CSD and the activation of the trigeminovascular system, which is known to be related to migraine pain, remains unclear.

Here, we investigated ERK phosphorylation in the trigeminal ganglion following both nociceptive stimulation of the dura mater and CSD using Western blot analysis and immunohistochemical methods. Our results provide evidence that CSD can activate dural TRPV1 receptors to send nociceptive signals to the trigeminal system.

2. Materials and methods

2.1. Animals

Experiments were performed on male Sprague-Dawley rats ($n=94$; body weight, 250–270 g), 20 of which were used for immunohistochemistry and the rest used for Western blot analysis. All experimental procedures were approved by the Animal Welfare Committee of Keio University (No. 08033). All procedures were undertaken with the utmost caution to minimize the suffering of the animals.

2.2. Experimental protocols

2.2.1. Temporal profile of capsaicin-induced ERK phosphorylation

The animals were deeply anesthetized by an intraperitoneal injection of pentobarbital sodium (30 mg/kg body weight). The head of each animal was fixed in a stereotaxic frame, and a burr hole (10 mm diameter) was made in the skull bone around the confluent sinus with the dura mater intact. A bank to prevent the spreading of the vehicle (10% ethanol in saline) or capsaicin solution was built around the burr hole using dental cement (Ionosit, DMG, Hamburg, Germany). Capsaicin was dissolved in 10% ethanol in saline. For control, we used the vehicle solution (10% ethanol in saline). To minimize the effect of the removal of the skull bone on the dural nociceptive nerve fibers, the surface of the dura mater surrounded by the dental cement was filled with saline, and the animal was kept anesthetized for 30 min. After these procedures, either the vehicle or 10 mM of capsaicin (8-methyl-*N*-vanillyl-trans-6-nonenamide, NO.M2028; Sigma, St. Louis, MO) was applied to the dura mater. The animals that received 3 min of saline were assigned to the control group. The capsaicin-treated animals were divided into three groups depending on the duration capsaicin administration: 1 min, 3 min, or 5 min. Each group contained 10 animals (6 animals were analyzed by Western blotting and 4 animals by immunohistochemistry). In addition, we observed longer effects of capsaicin on ERK phosphorylation: 15 min, 30 min, or 60 min (6 animals in each group for Western blotting).

2.2.2. Effects of TRPV1 receptor antagonist and MEK inhibitors on capsaicin-induced ERK phosphorylation

To examine the effects of a TRPV1 antagonist, 25 mM of capsazepine (N-[2-(4-chlorophenyl)ethyl]-1,3,4,5-tetrahydro-7,8-dihydroxy-2H-2-benzazepine-2-carbothioamide, No. C191-5MG; Sigma, St. Louis, MO) was applied to the dura mater immediately after the removal of the skull bone. 30 min later, the capsazepine was washed out with saline, and capsaicin was applied. After 3 min, the animals were sacrificed, and the trigeminal ganglia were removed and prepared as a homogenate for Western blot analysis.

We also investigated the effects of MAPK extracellular signal-regulated kinase (MEK) inhibitors on the phosphorylation of ERK. PD98059 (50 μM, #9900; Cell Signaling Technology, Beverly, MA) or U0126 (100 μM, #9903; Cell Signaling Technology, Beverly, MA) was applied to the dura mater for 30 min followed by capsaicin application and homogenate preparation (4 animals in each group).

2.2.3. Retrograde tracer experiment

A burr hole (10 mm in diameter) was made in the skull bone around the confluent sinus with the dura mater left intact. A bank was built around the burr hole using dental cement (Ionosit, DMG) to prevent the spreading of the tracer. A retrograde neuronal tracer, true blue (trans-1, 2-bis [5-amidino-2-benzofuranyl] ethylene-2HCl; Invitrogen) crystal (0.5 mg), was applied to the dura mater (4 animals). Following the application of the tracer, the application site was covered with the skull bone and dental cement.

Two weeks after the tracer application, the skull bone was removed again, and the dura mater where the tracer was applied was exposed. After a 3 min application of 10 mM capsaicin, the animals were perfused transcardially, and the trigeminal ganglia were dissected and processed for immunohistochemistry.

2.2.4. Effects of CSD on the phosphorylation of ERK

Male Sprague-Dawley rats were anesthetized with isoflurane (1.0% in room air with a flow rate of 400 mL/min) via a concentration-controllable anesthesia unit (400; Univentor, Zejtun, Malta). Body temperature was maintained with a heating pad and thermocontroller (BWT-100; Bioresearch Center Co., Nagoya, Japan). Each animal was fixed to a head-holder (SG-4N, modified to be flexible around the horizontal axis; Narishige Scientific Instrument Laboratory, Tokyo). For the measurement of DC potentials, an Ag/AgCl electrode (tip diameter = 200 μm, EEG-5002Ag; Bioresearch Center Co.) was inserted 200 μm under the pia mater (2 mm posterior and 2 mm lateral to bregma) and fixed with dental cement. Ag/AgCl reference electrodes (EER-5004Ag; Bioresearch Center Co.) were placed in the subcutaneous tissue. DC potentials were amplified at 1–100 Hz and digitized at 1 kHz with a differential headstage and differential extracellular amplifier (Models 4002 and EX1; Dagan Co., Minneapolis, MN). The DC electrodes were set on the bilateral exposed parietal cortex under anesthesia. We also installed small open cranial windows near each electrode for inducing CSD using a 1 M KCl solution. Animals were divided into three groups with 5 animals in each group. In the control group (group-1), saline was applied to the open cranial window instead of a 1 M KCl solution. In group-2, bilateral trigeminal ganglia were dissected immediately after the first wave of CSD. In group-3, the ganglia were removed 30 min after the first wave of CSD. In another experiment, animals were divided into two groups. In one group, capsazepine (50 nM) was injected into the cisterna magna (group-5). For the control group, vehicle (20% DMSO in saline) was injected instead of capsazepine (group-4). In group 4 and 5, capsazepine or vehicle was administrated 30 min before 1 M KCl application. In both groups, 1 M KCl was applied on the cranial window to induce CSD, and 30 min later, bilateral trigeminal ganglia were dissected. In both experiments, the specimens were prepared for Western blot analysis.

2.3. Western blot analysis

After the bilateral trigeminal ganglia were dissected, they were homogenized in ice-cold lysis buffer (20 mM Tris [pH 7.4], 2 mM EDTA, 20 mM glycerophosphate, 1 mM Na_3VO_4, 2 mM NaF, and complete protease inhibitor). The proteins were separated using 10% sodium dodecyl sulfate polyacrylamide gel electrophoresis (SDS-PAGE) and electrophoretically transferred to polyvinylidene difluoride membranes (Millipore Corporation). After treating with

a blocking solution containing 4% nonfat dry milk for 30 min, the membranes were incubated with an anti-phospho-p44/42 MAPK antibody (pERK, raised in rabbits [rabbit polyclonal], 1:1000, #9101; Cell Signaling Technology, Beverly, MA) or an anti-p44/42 MAPK antibody (ERK, raised in rabbits, 1:1000, #9102; Cell Signaling Technology, Beverly, MA) in blocking buffer overnight at 4 °C. Then, the membranes were washed with Tris-buffered saline containing 0.05% Tween-20 (TBS-T) and were incubated with horseradish peroxidase-conjugated goat anti-rabbit IgG (1:10,000; Jackson Immunoresearch Laboratories, West Grove, PA) for 2 h at room temperature. The immunoreactive bands were visualized using enhanced chemiluminescence and detected using a luminoimage analyzer (Las-4000; Fujifilm, Tokyo, Japan). The ratios of the intensities of phospho-ERK1 to total ERK1 and phospho-ERK2 to total ERK2 were calculated using the image analysis software Multi Gauge version 3.0 (Fujifilm, Tokyo, Japan). The ratios were normalized to the control samples and subjected to statistical analysis.

2.4. Immunohistochemical analysis

Animals in each group were transcardially perfused with 200 mL of 0.01 M phosphate-buffered saline (PBS, pH 7.2), followed by a mixture of 2% formaldehyde and 0.2% picric acid in a 0.01 M phosphate buffer, pH 7.0. Immediately after perfusion and fixation, the trigeminal ganglia were dissected. After cryoprotection, the specimens were processed into 7 μm-thick sections using a cryostat (Reichert-Jung Cryocut 1800; Leica Instruments, Heidelburg, Germany). For antigen retrieval, the slides were placed in boiling 0.01 M citrate buffer solution at pH 7.0 (Muto Pure Chemicals, Tokyo, Japan) for 10 min. After this procedure, the cryostat sections were preincubated with 10% normal donkey serum for 30 min. Then, the preincubated sections were incubated with the primary antibodies for 48–72 h at room temperature, washed with 0.01 M PBS, and subsequently incubated with species-specific secondary antibodies for 2 h at room temperature. The specimens were mounted in buffered glycerol (pH 8.6), and the slides were labeled with anti-phospho-p44/42 MAPK antibody (pERK, 1:1000). For double staining, the slides were double-labeled with anti-pERK antibody and anti-NeuN antibodies (raised in a mouse; code MAB 377; Millipore, Billerica, MA; 1:200). The immunoreactivities of the primary antibodies were visualized using species-specific secondary antibodies raised in donkeys and were conjugated to Cy3 or fluorescein isothiocyanate (FITC); all of the secondary antibodies were obtained from Jackson Immunoresearch Laboratories (West Grove, PA). For the retrograde tracing experiment, sections were labeled using anti-pERK and anti-TRPV1 (raised in a rabbit; code KM 018; TransGenic, Kumamoto, Japan; 1:200) antibodies. Secondary antibody conjugated to Cy3 and FITC were used to distinguish the immunolabeling from the labeling with true blue. The same immunostaining procedures were used for the control tissue sections with the omission of the primary antisera.

2.5. Quantitative analysis of immunohistochemistry and tracer experiments

The immunolabeled specimens were examined under an Olympus BX 50 microscope (Olympus, Tokyo, Japan) fitted with highly discriminating filters. Images from the BX 50 microscope were captured via a Sony CCD video camera (model XCD-SX 900; Sony, Tokyo, Japan) on an EPSON computer.

For quantitative immunohistochemical analysis, every third section was used. We analyzed the first 16 sections per ganglion, including the first branch of the trigeminal ganglionic neurons, because the superior sagittal sinus is known to be innervated by the ophthalmic division of the trigeminal ganglia. To calculate the ratio of pERK-immunoreactive (IR) neurons, we counted the total number of trigeminal ganglionic neurons and the number of pERK-IR neurons. With regard to the pERK-IR neurons, only those neurons that showed a clear increase in immunoreactivity above the background staining were counted. The total number of trigeminal ganglionic neurons with visible nuclei was obtained using a conventional light microscope. All of the areas of each section were randomly analyzed by two blinded observers. For the quantitative analysis of the tracer experiment in the trigeminal ganglion, we counted, from the top to the bottom, the number of true blue-containing neurons in every third section that contained nuclei. In addition, we counted the numbers of both pERK-IR and TRPV1-IR neurons showing an accumulation of the true blue tracer. Cross-sectional areas of the soma were determined using the image analyzing software of the BZ 9000 microscope (Keyence, Japan).

2.6. Statistical analysis

The data are presented as the mean ± SD and were compared using a Kruskal–Wallis one-way analysis of variance followed by a Mann–Whitney test for multiple comparisons (SPSS for Windows, version 21; SPSS Inc., Chicago, IL). The differences between the means were considered statistically significant at $p < 0.05$.

3. Results

3.1. Temporal profile of capsaicin-induced ERK phosphorylation in the trigeminal ganglion

To identify the temporal profile of ERK phosphorylation in the trigeminal ganglion, we stimulated the dura mater by a local application of a capsaicin solution. For the Western blot analysis, the antibody specific for the phosphorylated form of ERK identified two bands at molecular weights of 44 and 42 kDa, corresponding to phosphorylated ERK1 and ERK2, respectively. Representative blots of the trigeminal ganglion pERK and ERK are shown in Fig. 1A. In vehicle-treated animals, there was a basal level of phosphorylated ERK immunoreactivity that increased at 1 min and the peaked at 3 min after stimulation. The ratios of phosphorylated ERK/total ERK at 1, 3, and 5 min after capsaicin stimulation were 1.9 ± 1.2, 2.5 ± 1.1, and 2.3 ± 0.5 for ERK1 and 2.0 ± 0.6, 2.5 ± 0.7, and 2.1 ± 0.4 for ERK2, respectively (Fig. 1B and C). Although the level of phosphorylation had begun to decrease by 5 min, it still showed higher levels at 5 min. In particular, ERK1 exhibited a significantly higher level of phosphorylation at 5 min compared to controls. Therefore, we observed the levels of phosphorylation over a longer period of time following capsaicin stimulation. The ratios of phosphorylated ERK/total ERK at 15, 30, and 60 min after capsaicin stimulation were 1.5 ± 0.5, 1.4 ± 0.2, and 1.4 ± 0.3 for ERK1 and 1.6 ± 0.5, 1.3 ± 0.3, and 1.3 ± 0.3 for ERK2, respectively. These ratios were gradually decreased, and close to the basal level by 60 min.

Both ERK1 and ERK2 displayed significantly higher levels of phosphorylation at 3 min after capsaicin stimulation compared to the vehicle-treated controls. We also observed the levels of phosphorylation over a longer period of time following capsaicin stimulation. The ratios of phosphorylated ERK/total ERK at 15, 30, and 60 min after capsaicin stimulation were 1.5 ± 0.5, 1.4 ± 0.2, and 1.4 ± 0.3 for ERK1 and 1.6 ± 0.5, 1.3 ± 0.3, and 1.3 ± 0.3 for ERK2, respectively.

3.2. Attenuation of capsaicin-induced ERK activation using a TRPV1 receptor antagonist and MEK inhibitors

We next determined whether TRPV1 receptor stimulation and MEK activation mediated the capsaicin-induced ERK phosphorylation. As shown in Fig. 2A, the phosphorylation of ERK at 3 min after capsaicin application was attenuated in animals preincubated with

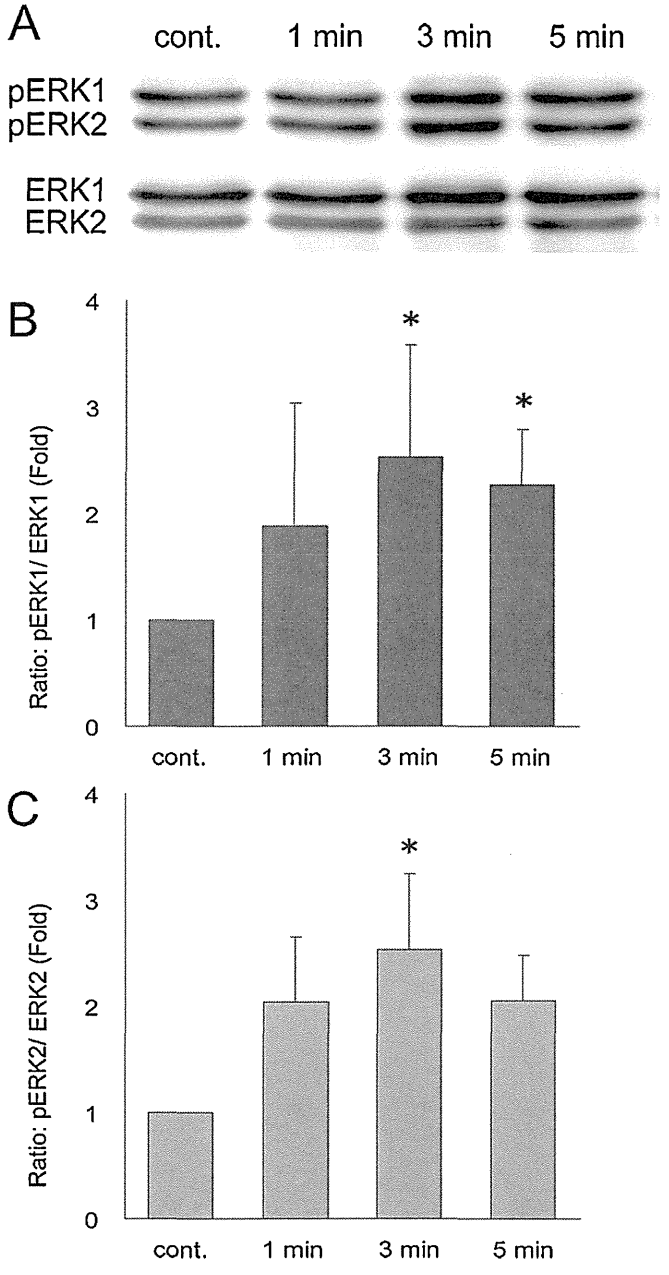

Fig. 1. Temporal profile of capsaicin-induced ERK phosphorylation in the trigeminal ganglion. Temporal profile of the phosphorylation of ERK1/2 in trigeminal ganglion neurons following the application of capsaicin to the dura mater. In vehicle-treated animals, the trigeminal ganglia were collected 3 min after vehicle stimulation of the dura mater; in capsaicin-treated animals, the specimens were collected at 1, 3, and 5 min. The time course for the phosphorylation of ERK1/2 was evaluated using Western blotting. A representative image is shown in (A), and the ratios of the intensities of pERK1 and pERK2 are shown in (B) and (C), respectively. A marked increase in the phosphorylation of ERK1/2 was observed 3 min after the application of capsaicin. The ratios of phosphorylated ERK1/2 to total ERK 1/2 were still higher levels at 5 min, and notably, ERK1 showed a significantly higher level of phosphorylation at 5 min compared to controls. (*$p < 0.05$; $n = 6$ in each group; error bars indicate SD).

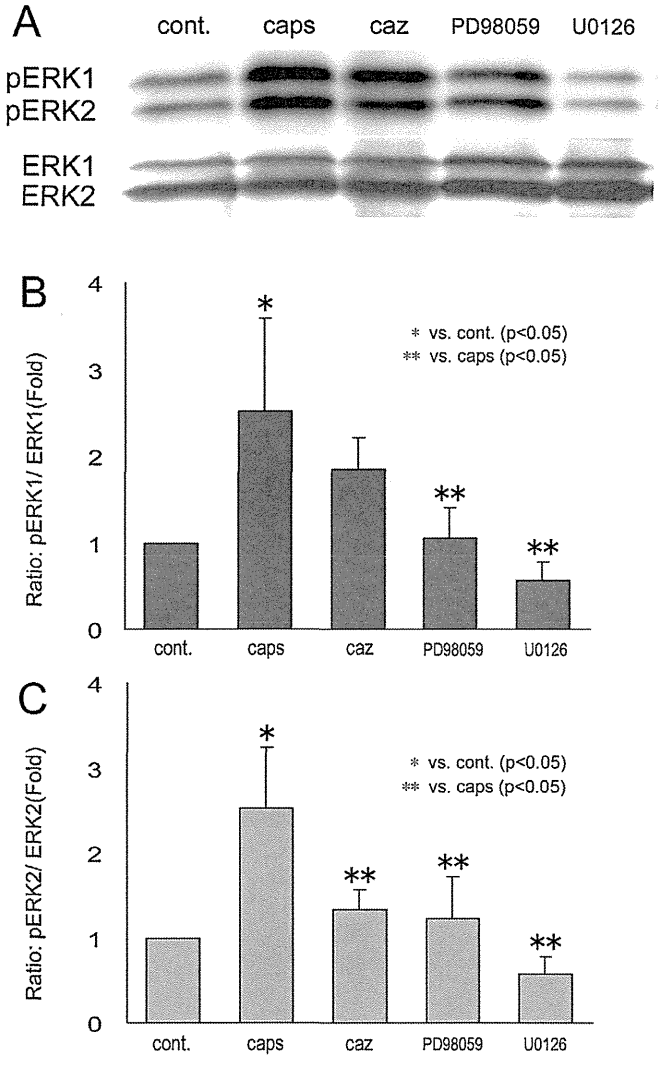

Fig. 2. Attenuation of capsaicin-induced ERK activation by a TRPV1 receptor antagonist and MEK inhibitors. Effects of TRPV1 receptor antagonist or MEK inhibitors on the phosphorylation of ERK1/2. Representative Western blot results are shown in (A), and the ratios of the intensities of pERK1/ERK1 and pERK2/ERK2 are shown in (B) and (C), respectively. For the control group (cont.), the vehicle was applied to the dura mater for 3 min. The designation "caps" indicates those animals in which capsaicin was applied to the dura mater for 3 min without preincubation with the TRPV1 receptor antagonist or MEK inhibitors. Significant increases in the ratios of the intensities of pERK1 and pERK2 were observed in the capsaicin-treated animals (caps) compared to those of the control group (cont). Conversely, the animal groups preincubated for 30 min with the TRPV1 receptor antagonist (caz) or MEK inhibitors (PD98059, U0126) exhibited decreased pERK1 and pERK2 ratios after the application of capsaicin to the dura mater compared to those of capsaicin-only-treated animals (caps). The phosphorylation of ERK1/2 was inhibited in animals preincubated with the TRPV1 receptor antagonist capsazepine; however, only ERK2 showed a significant difference between capsaicin-treated animals and animal groups preincubated with capsazepine (caz). Both MEK inhibitors, PD98059 and U0126, produced a significant decrease in the phosphorylation of ERK1/2 (* vs. control, $p < 0.05$; ** vs. capsaicin applied animals, $p < 0.05$; $n = 4$ in each group; error bars indicate SD).

capsazepine, a TRPV1 receptor antagonist (Fig. 2A, caz). In addition, the MEK inhibitors PD98059 and U0126 inhibited the phosphorylation of ERK at 3 min after capsaicin application (Fig. 2A, PD98059, U0126). The ratios of phosphorylated ERK/total ERK were 2.5 ± 1.1 (caps), 1.9 ± 0.4 (caz), 1.1 ± 0.4 (PD98059), and 0.6 ± 0.2 (U0126) for ERK1 and 2.5 ± 0.7 (caps), 1.3 ± 0.2 (caz), 1.2 ± 0.5 (PD98059), and 0.6 ± 0.2 (U0126) for ERK2 (Fig. 2B and C). The statistical analysis showed a significant decrease in ERK2 phosphorylation with capsazepine and the phosphorylation of both ERK1 and ERK2 with PD98059 or U0126 compared to the results obtained in the capsaicin-only-treated animals.

3.3. Immunohistochemical analysis of pERK in the trigeminal ganglion after dural nociceptive stimulation

We also performed an immunohistochemical analysis of phosphorylated ERK (pERK) using rat trigeminal ganglion slices. As

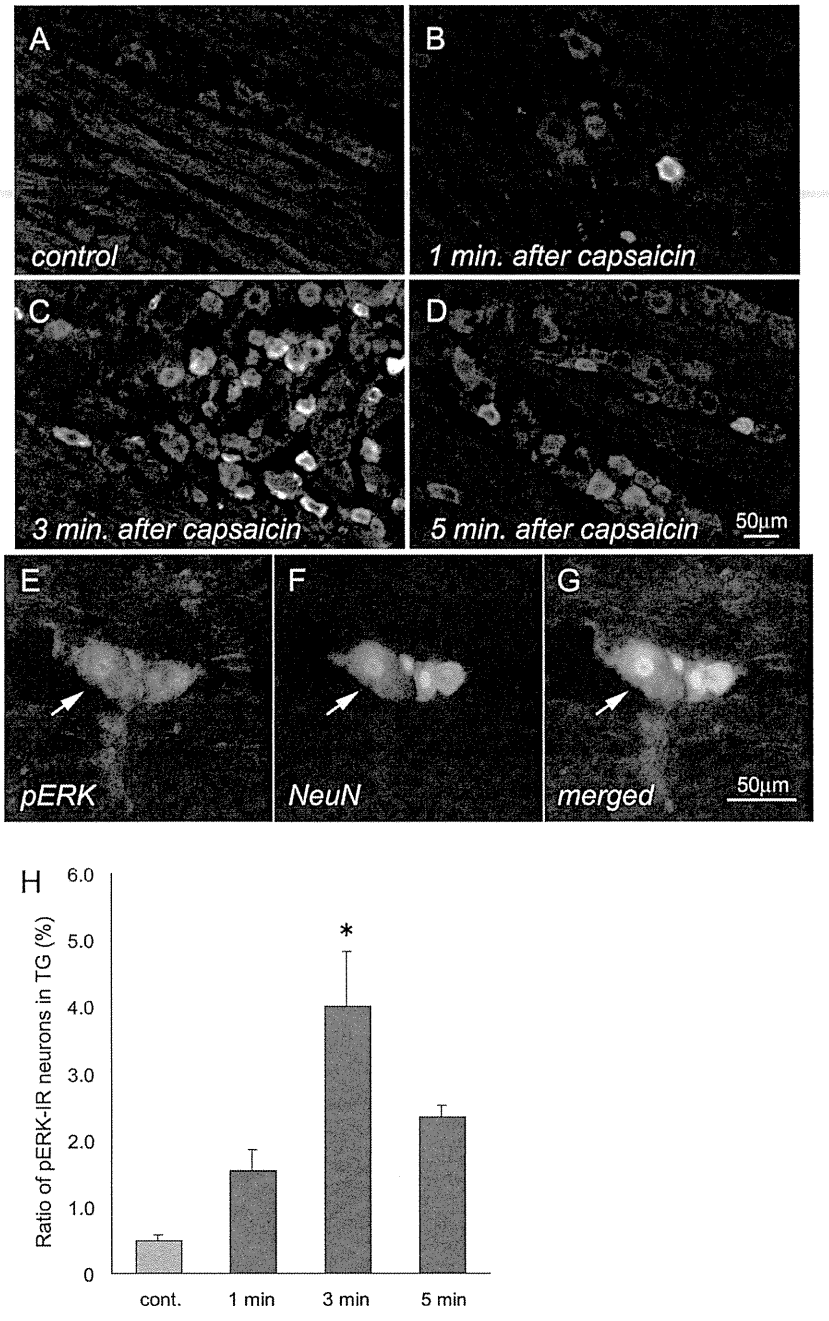

Fig. 3. Immunohistochemical analysis of pERK in the trigeminal ganglion following dural nociceptive stimulation. Immunohistochemical analysis of the time course of phosphorylation of ERK1/2 after the treatment of trigeminal ganglion neurons with capsaicin. (A–D) In the controls, few pERK-IR-exhibiting neurons were observed (A). At 1 min after the application of capsaicin, only a few pERK-IR-exhibiting neurons were observed (B). At 3 min, several neurons exhibited pERK-IR, after which pERK-IR labeling was subsequently decreased at 5 min (C and D; scale bar = 50 μm). (E–G): Double-labeling for pERK (red; E) and NeuN (green; F) immunoreactivity in the trigeminal ganglion 3 min after capsaicin stimulation. The arrow indicates a pERK-IR neuron co-localized with NeuN. (G) Merged image of (E) and (F). Scale bar = 50 μm. (H) Histogram summarizing the quantitative data for pERK-IR in the trigeminal ganglion (A–D). As shown in the histogram, the phosphorylation of ERK after capsaicin stimulation of the dura mater shows a temporal profile similar to that obtained by Western blot analysis (*$p < 0.05$; $n = 4$ in each group; error bars indicate SD).

shown in Fig. 3A, the vehicle-administered animals (controls) showed only a small number of pERK-immunoreactive (pERK-IR) cells. We observed only a few pERK-IR neurons at 1 min after capsaicin application (Fig. 3B), but the number increased 3 min after capsaicin application and was reduced at 5 min (Fig. 3C and D). Quantitatively, the proportion of pERK-IR cells was 0.6% among the control animals (5220 neurons from 4 animals). Following capsaicin administration, pERK immunoreactivity was detectable in 1.5% of all of the cells examined at 1 min after application (5927 neurons), 4.0% at 3 min (4054 neurons), and 2.3% at 5 min (8375 neurons). The ratios of the pERK-IR neurons at 3 min after capsaicin application differed significantly from those of the control animals (Fig. 3H). To demonstrate that ERK was phosphorylated in the neurons, we performed double immunostaining using anti-pERK and anti-NeuN antibodies. As shown in Fig. 3E and F, the immunoreactivity of pERK was restricted to NeuN-IR neurons. Control tissue sections lacking the primary antisera showed no specific staining patterns (data not shown).

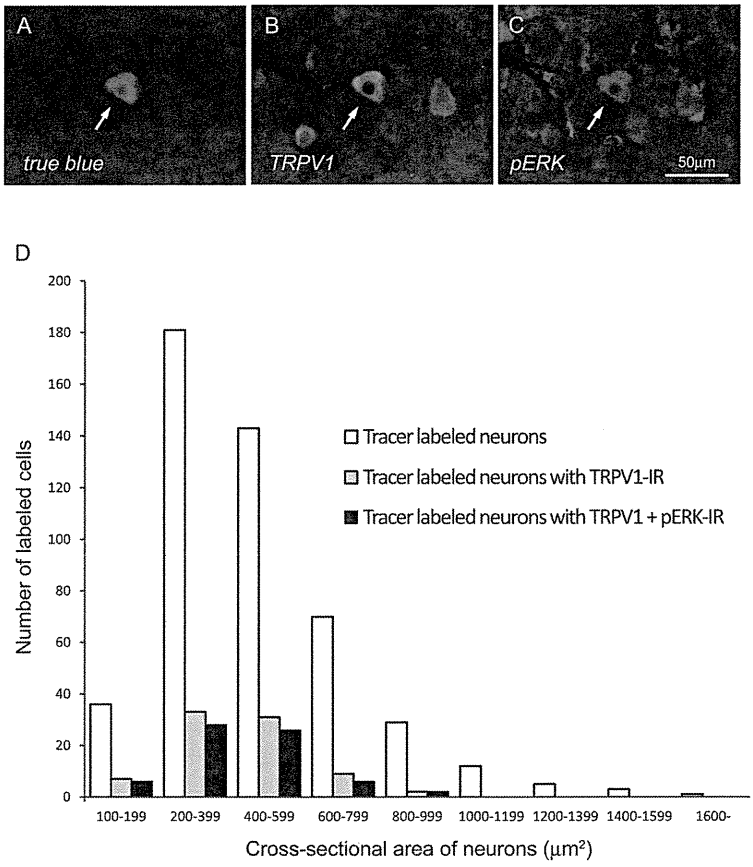

Fig. 4. The size of p-ERK-IR neurons with retrograde labeling. Sections of the trigeminal ganglion containing neurons retrogradely labeled with true blue (A), TRPV1-IR (B), and pERK-IR (C). Two weeks after administering the tracer, the skull bone was again removed, and capsaicin was applied to the dura mater. Neurons that retrogradely labeled with true blue (A) and co-localized with TRPV1-IR (B) and pERK-IR (C) are indicated by arrows. Scale bar, 50 μm for all. (D) The size distribution of retrogradely labeled neurons (open bars), retrogradely labeled neurons with TRPV1-IR (gray bars), and retrogradely labeled neurons with TRPV1 and pERK-IR (solid bars).

3.4. Combined use of a neuronal retrograde tracer technique and immunohistochemical analysis of pERK

Following the administration of true blue to the dura mater, retrogradely labeled neurons were observed in the bilateral trigeminal ganglion (Fig. 4A). Additionally, some of these retrogradely labeled neurons showed TRPV1- and pERK-IR (Fig. 4B and C). The mean cross-sectional area of the retrogradely labeled neurons was $478 \pm 250\ \mu m^2$ (mean ± SD; 4 animals, 480 neurons). The mean cross-sectional area of soma labeling for pERK and TRPV1 containing the retrogradely labeled neurons was $414 \pm 171\ \mu m^2$ (mean ± SD; 4 animals, 68 neurons) and was significantly smaller compared to that of the retrogradely labeled neurons ($p < 0.05$). A total of 20% of the neurons that accumulated the tracer showed TRPV1-IR, and 83% of those neurons exhibited pERK-IR. The size distributions of all retrogradely labeled neurons, retrogradely labeled neurons with TRPV1-IR and retrogradely labeled neurons with TRPV1 and pERK-IR were calculated. As shown in Fig. 4D and Table 1, the area of most of the neurons retrogradely labeled with TRPV1 and pERK-IR was between 200 and $600\ \mu m^2$ (arrows in Fig. 4A–C). Although some large neurons with tracer accumulation were observed, no neurons showing TRPV1-IR had an area of over $1000\ \mu m^2$.

3.5. Effects of CSD on the phosphorylation of ERK in the trigeminal ganglion of rat

Representative blots for pERK and ERK in the trigeminal ganglion are shown in Fig. 5A and D. The ratios of pERK/total-ERK were 1.82 ± 0.48 for ERK1 and 2.97 ± 0.76 for ERK2 in group-3; 1.12 ± 0.45 for ERK1 and 1.24 ± 0.63 for ERK2 in group-2. The ratios of pERK/total-ERK showed significantly higher levels in group-3 compared to group-1 ($p < 0.05$); however, there was no significant difference between group-1 and group-2 (Fig. 5B and C).

The ratios of pERK/total-ERK were 0.23 ± 0.35 for ERK1 and 0.35 ± 0.43 for ERK2 in group-5. The ratios of pERK/total-ERK showed significantly attenuated levels in group-5 compared to group-4 ($p < 0.05$; Fig. 5E and F). The frequencies of CSD occurrence during the 30 min were 4.7 ± 0.5 times in group-4 and 4.7 ± 1.4 times in group-5, and there was no significant difference between group-4 and group-5.

4. Discussion

4.1. Temporal profile of ERK phosphorylation resulting from dural nociceptive stimulation

Since Ji and colleagues first reported the involvement of ERK following the nociceptive stimulation of spinal neurons (Ji et al., 1999), many studies involving the stimulation (e.g., chemical, electrical, or mechanical) of peripheral C-fibers have shown ERK phosphorylation in the spinal cord, trigeminal nucleus, and dorsal root ganglion (Dai et al., 2002; Shimizu et al., 2006; Noma et al., 2008). Among these reports was a study by Dai and co-workers, who investigated the phosphorylation status of ERK during the very early stages immediately following TRPV1 stimulation. They observed a transient upregulation of ERK phosphorylation only minutes after TRPV1 stimulation in the dorsal root ganglion, which returned to

Table 1
Size distribution of all retrogradely labeled neurons and those retrogradely labeled neurons showing TRPV1- and p-ERK-IR.

Cross-sectional area of neurons (μm^2)	Number of retrogradely labeled cells	Number of cells retrogradely labeled with TRPV1-IR	Number of cells retrogradely labeled with TRPV1 and pERK-IR	Ratio of retrogradely labeled cells with TRPV1 and pERK-IR (%)
100–199	36	7	6	16.7
200–399	181	33	28	15.5
400–599	143	31	26	18.2
600–799	70	9	6	8.6
800–999	29	2	2	6.9
1000–1199	12	0	0	0
1200–1399	50	0	0	0
1400–1599	3	0	0	0
1600≤	1	0	0	0

baseline by 120 min (Dai et al., 2002). Our study shows a similar time course in terms of the upregulation of ERK phosphorylation after dural stimulation. We also observed ERK phosphorylation 60 min after dural stimulation and found that the upregulation of ERK phosphorylation gradually decreased to baseline levels. This time course of ERK phosphorylation is consistent with our in vitro experiment, which also demonstrated the translocation of pERK to the nucleus (supplementary data). These results imply a role for ERK, which translocates to the nucleus from the cytosol, in the regulation of gene expression.

Our study shows that the dural application of MEK inhibitors attenuated ERK phosphorylation at 3 min following the application of capsaicin. A previous study by Dai and colleagues demonstrated that intradermal administration of a MEK inhibitor prevented the increase of pERK-IR in peripheral nerve terminals and fibers of the skin after capsaicin stimulation, indicating the possibility that the activation of the ERK signaling pathway occurred within the nerve terminals and fibers in addition to the cell bodies in response to peripheral receptor stimulation (Dai et al., 2002). Furthermore, an increase in the expression of pERK in dural nerve fibers was reported after dural mast cell degradation (Levy et al., 2007). Based on these findings, it is likely that the phosphorylation of ERK primarily occurs at the nerve terminals with subsequent propagation to the soma.

We used the right and left side of the trigeminal ganglia for analysis. This methodology is based on our preliminary observations, which have indicated a similar degree of ERK phosphorylation in the bilateral trigeminal ganglia following the stimulation of dural TRPV1 receptors. These findings are also consistent with our tracer experiment, which shows the accumulation of the retrograde tracer in the bilateral trigeminal ganglion after its application to the dura mater around the confluent sinus.

4.2. Size of the neurons in the trigeminal ganglion showing ERK phosphorylation following dural nociceptive stimulation

In line with the findings of our Western blot analysis, immunohistochemical studies also demonstrated peak ERK phosphorylation 3 min after the dural application of capsaicin. To clarify the size of the trigeminal ganglionic neurons responding to dural nociceptive stimulation, we applied a retrograde tracer to the dura mater prior to administering the stimulus and then collected the immunohistochemical data 3 min later. Although the accumulation of the tracer was observed in neurons of varying sizes, most of the labeled neurons that showed TRPV1-IR were small-sized (area <600 μm^2), which includes neurons known to be related to thermal sensation and nociception (Gardner et al., 2000). This result is consistent with our previous results showing that TRPV1-IR neurons that are distributed in the dura mater are also small-sized neurons in the trigeminal ganglion (Shimizu et al., 2007). In addition, our immunohistochemical analysis, which examined the co-localization of pERK and TRPV1 revealed that most of these TRPV1-IR neurons that innervate the dura mater exhibit pERK-IR. Taken together, this study verifies that the nociceptive stimulation of the dura mater leads to the phosphorylation of ERK in small-sized neurons of the trigeminal ganglion.

4.3. Effects of CSD on the phosphorylation of ERK in the trigeminal ganglion

This study revealed that CSD affects the nociceptive stimulation to the trigeminal ganglion. It has been thought that CSD and the activation of the trigeminovascular system play important roles in the mechanism of migraines. Although CSD has been reported to be related to the pathophysiology of the migraine aura, it is still controversial whether CSD activates the trigeminovascular system. Zhang et al. reported that the trigeminal ganglion was activated at 14–25 min after CSD, and these temporal profiles in terms of the activation of the trigeminal ganglion after CSD were consistent with the results of this study (Zhang et al., 2010). Although the reason for the delay between the induction of CSD and the activation of the trigeminal ganglion system was unclear, this delay could explain why migraine headaches occur after the aura. Karatas et al. reported that CSD activates neuronal pannexin 1 channels, initiates inflammatory responses and promotes the sustained release of inflammatory mediators (Karatas et al., 2013). These inflammatory mediators are continuously released into the subarachnoid space via astrocytes forming the glia limitans and stimulate trigeminal nerve endings around pial vessels. Kosaras et al. revealed that these trigeminal nerve fibers innervating the pial vessels were connected to the dura mater by traversing the arachnoid space (Kosaras et al., 2009). These anatomical findings make it possible to explain the activation of the trigeminal ganglion following CSD.

More importantly, our pharmacological study has raised the possibility that TRPV1 mediates the CSD-induced nociceptive signaling to the trigeminal system (Fig. 6). In animal experiments, CSD is known to evoke a transient release of excitatory amino acids and to increase the extracellular level of proton, which is one of the agonists of TRPV1 (Levy, 2012). Furthermore, CSD is reported to cause degranulation of mast cells in the dura mater (Karatas et al., 2013). The mast cells contain serotonin, histamine and prostaglandin E_2 (Bergerot et al., 2000; Zimmermann et al., 2003), and these substances are known to induce TRPV1 sensitization, which decreases the threshold of TRPV1 activation in terms of temperature and acidity (Sugiura et al., 2002; Dux et al., 2012). Taken together, CSD causes the sensitization and activation of TRPV1, and increases the level of the phosphorylation of ERK.

The ERK signal transduction pathways were originally identified as the primary effectors of growth factor receptor such as TrkA.

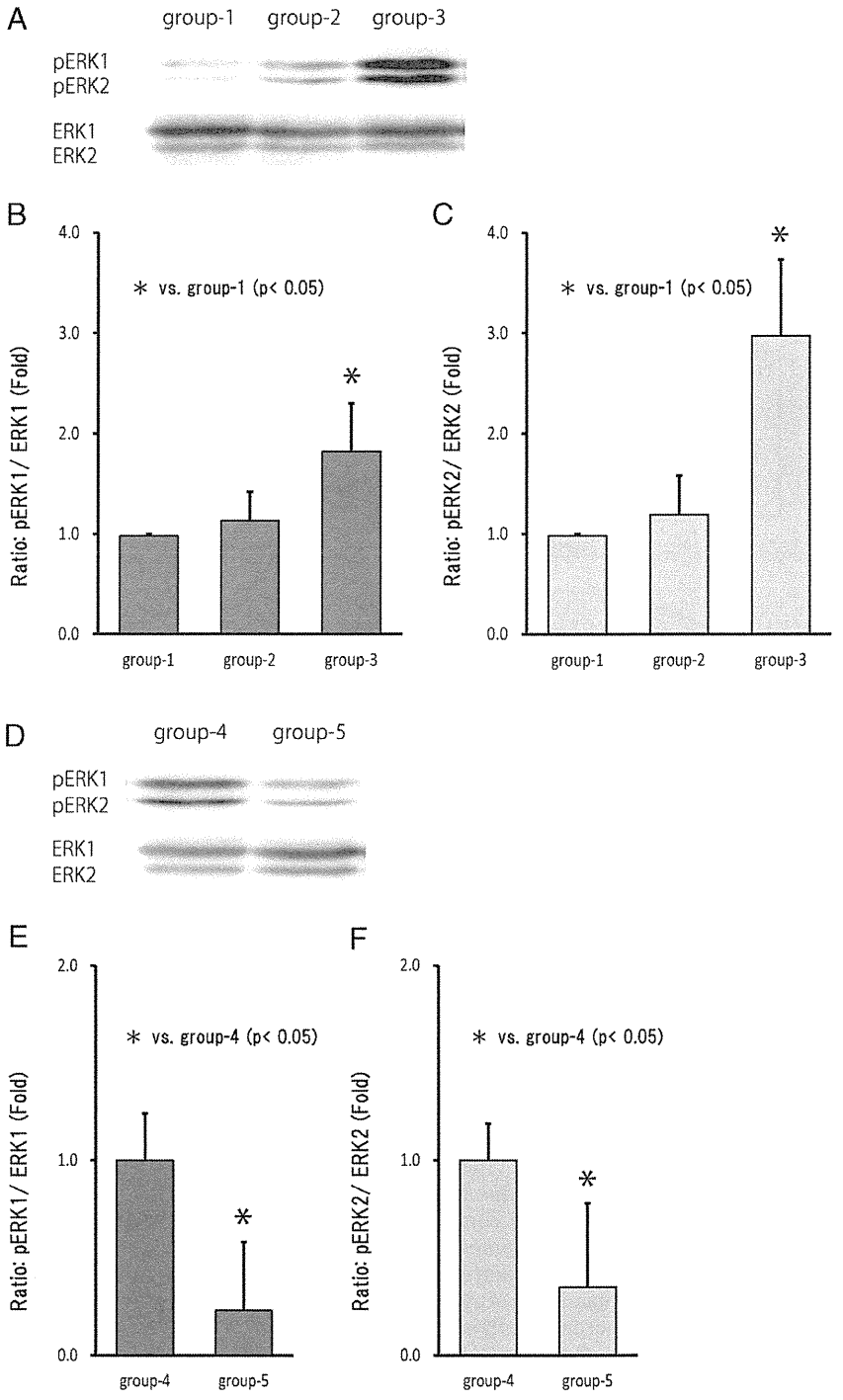

Fig. 5. Effects of CSD on ERK activation. The level of phosphorylation of ERK1/2 in trigeminal ganglion neurons following CSD. In group-2, bilateral trigeminal ganglia were dissected immediately after the first wave of CSD. In group-3, they were removed 30 min after the first wave of CSD. In group-1 (control), saline was applied to the open cranial window instead of the 1 M KCl solution used to evoke CSD. A representative image is shown in (A), and the ratios of the intensities of pERK1 and pERK2 are shown in (B) and (C), respectively. A marked increase in the phosphorylation of ERK1/2 was observed in group-3 compared to control (*$p < 0.05$; $n = 5$ in each group; error bars indicate SD). In another experiment, capsazepine (50 nM) was injected into the cisterna magna (group-5). In group-4, vehicle (20% DMSO in saline) was injected instead of capsazepine. In both groups, 1 M KCl was applied to the cranial window to induce CSD, and 30 min later, the bilateral trigeminal ganglia were dissected for Western blot analysis. A representative image is shown in (D), and the ratios of the intensities of pERK1 and pERK2 are shown in (E) and (F), respectively. A marked decrease in the phosphorylation of ERK1/2 was observed in group-5 compared to group-4 (*$p < 0.05$; $n = 5$ in each group; error bars indicate SD).

In this pathway, after GTP loading and activation of the small G-protein Ras were provoked by activated receptors, Ras-GTP recruits a three-tiered enzyme cascade in which a MAPK kinase (Raf) phosphorylates MEK, which phosphorylates and activates ERK (English et al., 1999). Although the precise pathway for the ERK signal transduction responsible for nociceptive stimulation is still obscure, the activation of the NMDA receptor or voltage-gated calcium channels such as TRPV1 is considered to cause calcium influx or release from intracellular stores, and activates several calcium-dependent kinases in the ERK signal transduction pathway,

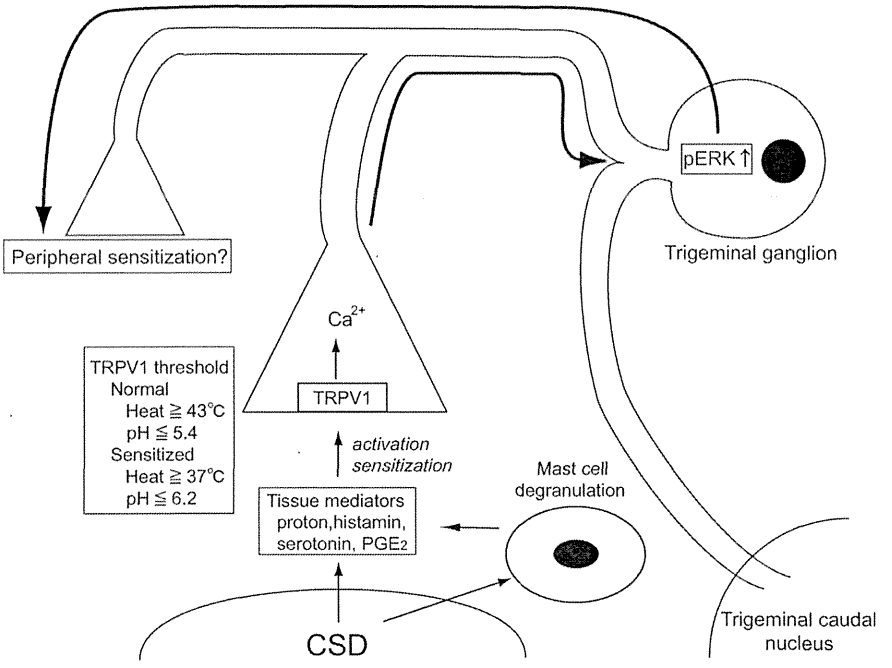

Fig. 6. Schematic representation for the possible relationship between CSD and the phosphorylation of ERK via TRPV1 activation. CSD causes a transient release of excitatory amino acids and to increase the extracellular level of proton. Furthermore, CSD facilitates degranulation of mast cells in the dura mater. The mast cells contain serotonin, histamine and prostagrandin E_2, and these substances are known to induce TRPV1 sensitization, which decreases the threshold of TRPV1 activation by temperature and proton. Influx of Ca^{2+} via TRPV1 increases the level of the phosphorylation of ERK, and it may cause peripheral hypersensitivity via transcriptional regulation.

including protein kinase C, tyrosine kinase, calcium/calmodulin-dependent kinase, adenylate cyclase and tyrosine kinase Pyk2, leading to ERK phosphorylation (Ji and Woolf, 2001; Obata and Noguchi, 2004).

As previously described, recent studies revealed the relationship between ERK phosphorylation and sensitization of the trigeminal ganglion (Yan et al., 2012; Zhang et al., 2013). Since the results of this experiment exhibited the potentiation of the level of the phosphorylation of ERK in the trigeminal ganglion after CSD, our data indicate the possibility that CSD may contribute to migraine-related sensitization.

In clinical studies, Diamond et al. have been reported the efficaciousness of civamide, which is a TRPV1 agonist, for the acute treatment of migraine headache (Diamond et al., 2000). They presumed that the anti-migraine action of civamide was due to desensitization of TRPV1 function. Their finding conferred clinical evidence for the involvement of TRPV1 in the development of migraine headache. Furthermore, Evans et al. have reported that sumatriptan, which is one of the effective migraine abortive drugs, inhibits TRPV1 channels in trigeminal neurons, implying that TRPV1 plays an important role in the migraine-aborting action of sumatriptan (Evans et al., 2012). In addition to these findings, our results imply a pivotal role of TRPV1 for the pathophysiology of migraine, and provide an important clue to novel therapeutic strategies against migraine.

5. Conclusions

The present findings demonstrate that the nociceptive stimulation of TRPV1 receptors in the dura mater causes the phosphorylation of ERK in small-sized neurons of the trigeminal ganglion. CSD also induces the phosphorylation of ERK via TRPV1 stimulation in the trigeminal ganglion. These results indicate the possibility that CSD may act to provide nociceptive stimulation to the trigeminal ganglion and provide important clues regarding the relationship between CSD and the activation of the trigeminovascular system.

Conflict of interest statement

The authors have no conflicts of interest to declare.

Acknowledgements

This research was supported in part by a Grant-in-Aid for Scientific Research (grant number 22390182 to N. Suzuki) from the Ministry of Education, Culture, Sports, Science and Technology of Japan.

Appendix A. Supplementary data

Supplementary data associated with this article can be found, in the online version, at http://dx.doi.org/10.1016/j.neures.2013.08.001.

References

Andres, K.H., von During, M., Muszynski, K., Schmidt, R.F., 1987. Nerve fibres and their terminals of the dura mater encephali of the rat. Anat. Embryol. (Berl.) 175, 289–301.

Bergerot, A., Reynier-Rebuffel, A.M., Callebert, J., Aubineau, P., 2000. Long-term superior cervical sympathectomy induces mast cell hyperplasia and increases histamine and serotonin content in the rat dura mater. Neuroscience 96, 205–213.

Dai, Y., Iwata, K., Fukuoka, T., Kondo, E., Tokunaga, A., Yamanaka, H., Tachibana, T., Liu, Y., Noguchi, K., 2002. Phosphorylation of extracellular signal-regulated kinase in primary afferent neurons by noxious stimuli and its involvement in peripheral sensitization. J. Neurosci. 22, 7737–7745.

Diamond, S., Freitag, F., Phillips, S.B., Bernstein, J.E., Saper, J.R., 2000. Intranasal civamide for the acute treatment of migraine headache. Cephalalgia 20, 597–602.

Dux, M., Santha, P., Jancso, G., 2012. The role of chemosensitive afferent nerves and TRP ion channels in the pathomechanism of headaches. Pflugers Arch. 464, 239–248.

English, J., Pearson, G., Wilsbacher, J., Swantek, J., Karandikar, M., Xu, S., Cobb, M.H., 1999. New insights into the control of MAP kinase pathways. Exp. Cell Res. 253, 255–270.

Evans, M.S., Cheng, X., Jeffry, J.A., Disney, K.E., Premkumar, L.S., 2012. Sumatriptan inhibits TRPV1 channels in trigeminal neurons. Headache 52, 773–784.

Gardner, E.P., Martin, J.H., Jessell, T.M., 2000. The bodily senses. In: Kandel, E.R., Schwartz, J.H., Jessell, T.M. (Eds.), Principles of neural science. , Fourth edition. McGraw-Hill, New York, pp. 430–450.

Hadjikhani, N., Sanchez Del Rio, M., Wu, O., Schwartz, D., Bakker, D., Fischl, B., Kwong, K.K., Cutrer, F.M., Rosen, B.R., Tootell, R.B., Sorensen, A.G., Moskowitz, M.A., 2001. Mechanisms of migraine aura revealed by functional MRI in human visual cortex. Proc. Natl. Acad. Sci. U.S.A. 98, 4687–4692.

Ji, R.R., Woolf, C.J., 2001. Neuronal plasticity and signal transduction in nociceptive neurons: implications for the initiation and maintenance of pathological pain. Neurobiol. Dis. 8, 1–10.

Ji, R.R., Baba, H., Brenner, G.J., Woolf, C.J., 1999. Nociceptive-specific activation of ERK in spinal neurons contributes to pain hypersensitivity. Nat. Neurosci. 2, 1114–1119.

Ji, R.R., Gereau, R.W.t., Malcangio, M., Strichartz, G.R., 2009. MAP kinase and pain. Brain Res. Rev. 60, 135–148.

Karatas, H., Erdener, S.E., Gursoy-Ozdemir, Y., Lule, S., Eren-Kocak, E., Sen, Z.D., Dalkara, T., 2013. Spreading depression triggers headache by activating neuronal Panx1 channels. Science 339, 1092–1095.

Kosaras, B., Jakubowski, M., Kainz, V., Burstein, R., 2009. Sensory innervation of the calvarial bones of the mouse. J. Comp. Neurol. 515, 331–348.

Leão, A.A.P., 1944. Spreading depression of activity in the cerebral cortex. J. Neurophysiol. 7B, 359–390.

Levy, D., 2012. Endogenous mechanisms underlying the activation and sensitization of meningeal nociceptors: the role of immuno-vascular interactions and cortical spreading depression. Curr. Pain Headache Rep. 16, 270–277.

Levy, D., Burstein, R., Kainz, V., Jakubowski, M., Strassman, A.M., 2007. Mast cell degranulation activates a pain pathway underlying migraine headache. Pain 130, 166–176.

Messlinger, K., Hanesch, U., Baumgartel, M., Trost, B., Schmidt, R.F., 1993. Innervation of the dura mater encephali of cat and rat: ultrastructure and calcitonin gene-related peptide-like and substance P-like immunoreactivity. Anat. Embryol. (Berl.) 188, 219–237.

Noma, N., Tsuboi, Y., Kondo, M., Matsumoto, M., Sessle, B.J., Kitagawa, J., Saito, K., Iwata, K., 2008. Organization of pERK-immunoreactive cells in trigeminal spinal nucleus caudalis and upper cervical cord following capsaicin injection into oral and craniofacial regions in rats. J. Comp. Neurol. 507, 1428–1440.

Obata, K., Noguchi, K., 2004. MAPK activation in nociceptive neurons and pain hypersensitivity. Life Sci. 74, 2643–2653.

Olesen, J., Burstein, R., Ashina, M., Tfelt-Hansen, P., 2009. Origin of pain in migraine: evidence for peripheral sensitisation. Lancet Neurol. 8, 679–690.

Olesen, J., Friberg, L., Olsen, T.S., Iversen, H.K., Lassen, N.A., Andersen, A.R., Karle, A., 1990. Timing and topography of cerebral blood flow, aura, and headache during migraine attacks. Ann Neurol. 28, 791–798.

Reuss, S., Riemann, R., Vollrath, L., 1992. Substance P- and calcitonin gene-related peptide-like immunoreactive neurons in the rat trigeminal ganglion – With special reference to meningeal and pineal innervation. Acta Histochem. 92, 104–109.

Roux, P.P., Blenis, J., 2004. ERK and p38 MAPK-activated protein kinases: a family of protein kinases with diverse biological functions. Microbiol. Mol. Biol. Rev. 68, 320–344.

Shimizu, K., Asano, M., Kitagawa, J., Ogiso, B., Ren, K., Oki, H., Matsumoto, M., Iwata, K., 2006. Phosphorylation of extracellular signal-regulated kinase in medullary and upper cervical cord neurons following noxious tooth pulp stimulation. Brain Res. 1072, 99–109.

Shimizu, T., Toriumi, H., Sato, H., Shibata, M., Nagata, E., Gotoh, K., Suzuki, N., 2007. Distribution and origin of TRPV1 receptor-containing nerve fibers in the dura mater of rat. Brain Res. 1173, 84–91.

Sugiura, T., Tominaga, M., Katsuya, H., Mizumura, K., 2002. Bradykinin lowers the threshold temperature for heat activation of vanilloid receptor 1. J. Neurophysiol. 88, 544–548.

Uddman, R., Hara, H., Edvinsson, L., 1989. Neuronal pathways to the rat middle meningeal artery revealed by retrograde tracing and immunocytochemistry. J. Auton. Nerv. Syst. 26, 69–75.

Yan, J., Melemedjian, O.K., Price, T.J., Dussor, G., 2012. Sensitization of dural afferents underlies migraine-related behavior following meningeal application of interleukin-6 (IL-6). Mol. Pain 8, 6.

Zhang, X., Kainz, V., Zhao, J., Strassman, A.M., Levy, D., 2013. Vascular extracellular signal-regulated kinase mediates migraine-related sensitization of meningeal nociceptors. Ann. Neurol. 73, 741–750.

Zhang, X., Levy, D., Noseda, R., Kainz, V., Jakubowski, M., Burstein, R., 2010. Activation of meningeal nociceptors by cortical spreading depression: implications for migraine with aura. J. Neurosci. 30, 8807–8814.

Zimmermann, K., Reeh, P.W., Averbeck, B., 2003. S+-flurbiprofen but not 5-HT1 agonists suppress basal and stimulated CGRP and PGE2 release from isolated rat dura mater. Pain 103, 313–320.

Neuroscience 248 (2013) 345–358

DIFFERENTIAL CELLULAR LOCALIZATION OF ANTIOXIDANT ENZYMES IN THE TRIGEMINAL GANGLION

H. SATO,[a,b,e] M. SHIBATA,[a*] T. SHIMIZU,[a] S. SHIBATA,[c] H. TORIUMI,[a] T. EBINE,[a] T. KUROI,[a] T. IWASHITA,[a] M. FUNAKUBO,[a] Y. KAYAMA,[a] C. AKAZAWA,[d] K. WAJIMA,[b] T. NAKAGAWA,[b] H. OKANO[c] AND N. SUZUKI[a]

[a] *Department of Neurology, School of Medicine, Keio University, 35 Shinanomachi, Shinjuku-ku, Tokyo 160-8582, Japan*

[b] *Department of Dentistry and Oral Surgery, School of Medicine, Keio University, 35 Shinanomachi, Shinjuku-ku, Tokyo 160-8582, Japan*

[c] *Department of Physiology, School of Medicine, Keio University, 35 Shinanomachi, Shinjuku-ku, Tokyo 160-8582, Japan*

[d] *Department of Biochemistry and Biophysics, Graduate School of Health and Sciences, Tokyo Medical and Dental University, 1-5-45 Yushima, Bunkyo-ku, Tokyo 113-8510, Japan*

[e] *Japan Society for the Promotion of Science, 8 Ichiban-cho, Chiyoda-ku, Tokyo 102-8472, Japan*

Abstract—Because of its high oxygen demands, neural tissue is predisposed to oxidative stress. Here, our aim was to clarify the cellular localization of antioxidant enzymes in the trigeminal ganglion. We found that the transcriptional factor Sox10 is localized exclusively in satellite glial cells (SGCs) in the adult trigeminal ganglion. The use of transgenic mice that express the fluorescent protein Venus under the *Sox10* promoter enabled us to distinguish between neurons and SGCs. Although both superoxide dismutases 1 and 2 were present in the neurons, only superoxide dismutase 1 was identified in SGCs. The enzymes relevant to hydrogen peroxide degradation displayed differential cellular localization, such that neurons were endowed with glutathione peroxidase 1 and thioredoxin 2, and catalase and thioredoxin 2 were present in SGCs. Our immunohistochemical finding showed that only SGCs were labeled by the oxidative damage marker 8-hydroxy-2′-deoxyguanosine, which indicates that the antioxidant systems of SGCs were less potent. The transient receptor potential vanilloid subfamily member 1 (TRPV1), the capsaicin receptor, is implicated in inflammatory hyperalgesia, and we demonstrated that topical capsaicin application causes short-lasting mechanical hyperalgesia in the face. Our cell-based assay revealed that TRPV1 agonist stimulation in the presence of TRPV1 overexpression caused reactive oxygen species-mediated caspase-3 activation. Moreover, capsaicin induced the cellular demise of primary TRPV1-positive trigeminal ganglion neurons in a dose-dependent manner, and this effect was inhibited by a free radical scavenger and a pancaspase inhibitor. This study delineates the localization of antioxidative stress-related enzymes in the trigeminal ganglion and reveals the importance of the pivotal role of reactive oxygen species in the TRPV1-mediated caspase-dependent cell death of trigeminal ganglion neurons. Therapeutic measures for antioxidative stress should be taken to prevent damage to trigeminal primary sensory neurons in inflammatory pain disorders.

Key words: trigeminal ganglion, glutathione peroxidase, catalase, transient receptor potential vanilloid subfamily member 1, caspase, inflammatory pain.

INTRODUCTION

Reactive oxygen species (ROS) are defined as oxygen-containing chemicals that are damaging to cellular components, such as lipids, proteins and nucleic acids. Oxidative stress stems from an imbalance in the generation and disposal of ROS, which leads to an elevated intracellular concentration of ROS and also leads to oxidative cell damage (Dringen et al., 2005). A superoxide anion ($O_2^{\cdot -}$) is generated, primarily by the mitochondrial respiratory chain and by cellular oxidases. The superoxide anion is quickly converted to hydrogen peroxide (H_2O_2) and oxygen by mitochondrial superoxide dismutase 1 (SOD1, Mn-SOD) and cytoplasmic SOD2 (Cu/Zn-SOD). H_2O_2 is degraded by several peroxide-decomposing enzyme systems, which include catalase, glutathione peroxidase (GPx) and the thioredoxin (Trx)/peroxiredoxin system (Salvemini et al., 2011). Of these systems, GPx1, a member of the GPx family, is known to play a major role in peroxide degradation in neural cells (Mitozo et al., 2011). Recent studies indicate that significant analgesic effects in both neuropathic pain (Khalil et al., 1999; Kim et al., 2004, 2010; Mao et al., 2009; Yowtak et al., 2011) and inflammatory pain (Thiemermann, 2003; Mika et al., 2007; Kuhad et al., 2008) are produced by the removal

*Corresponding author. Tel: +81-3-5363-3788; fax: +81-3-3353-1272.
E-mail address: mshibata@a7.keio.jp (M. Shibata).

Abbreviations: 8-OHdG, 8-hydroxy-2′-deoxyguanosine; ANOVA, analysis of variance; BAC, bacterial artificial chromosome; DMEM, Dulbecco's modified Eagle medium; EGFP, enhanced green fluorescent protein; flTRPV1, full-length TRPV1; GAPDH, glyceraldehyde 3-phosphate dehydrogenase; GLAST, glutamate/aspartate transporter; GPx, glutathione peroxidase; GST, glutathione S-transferase; HIV, human immunodeficiency virus; H_2O_2, hydrogen peroxide; HRP, horse radish peroxidase; JNK, c-Jun N-terminal kinase; $O_2^{\cdot -}$, superoxide anion; PBS, phosphate-buffered saline; Prx, peroxiredoxin; ROS, reactive oxygen species; RT-PCR, reverse transcription-polymerase chain reaction; SGCs, satellite glial cells; SOD, superoxide dismutase; STS, staurosporine; TBS-T, Tris-buffered saline/0.1% Tween-20; TEMPOL, 4-hydroxy-2,2,6,6-four methys piperidine; TG, trigeminal ganglion; TRPV1, transient receptor potential vanilloid subfamily member 1; Trx, thioredoxin.

0306-4522/13 $36.00
http://dx.doi.org/10.1016/j.neuroscience.2013.06.010

of excess ROS by free radical scavengers. Either systemic or intrathecal administration of ROS scavengers assuaged hyperalgesia that was induced by a formalin injection (Hacimuftuoglu et al., 2006) and mechanical allodynia in neuropathic pain models (Khalil et al., 1999; Kim et al., 2004), implying that the site of algogenic ROS production was within the peripheral nervous system (Kim et al., 2004). The trigeminal ganglia (TG) harbor trigeminal primary neurons, and intraganglionic modifications of nociceptive signals have been described (Rappaport and Devor, 1994; Ceruti et al., 2011). In addition to primary sensory neurons, many specialized glial cells, termed satellite glial cells (SGCs), are present in TG (Hanani, 2010). Similar to TG neurons and Schwann cells, SGCs are derived from the neural crest (Maro et al., 2004). Morphologically, SGCs surround the neurons and form an envelope-like structure that ensheaths the neurons. Because of their small size and the relative paucity of specific markers, not much attention has been paid to these glial cells until recently. Nevertheless, evidence is now accumulating that shows that SGCs play important modulatory roles in the development of pain disorders (Takeda et al., 2009; Katagiri et al., 2012).

The capsaicin receptor, TRPV1 (transient receptor vanilloid subfamily, member 1), is a non-selective cation channel and serves as a transducer of various stimuli into pain signals in the nociceptors (Tominaga et al., 1998; Caterina et al., 2000; Khairatkar-Joshi and Szallasi, 2009). TRPV1 function is upregulated by inflammatory mediators using posttranslational mechanisms, which are critically implicated in the development of inflammatory hyperalgesia (Davis et al., 2000; Khairatkar-Joshi and Szallasi, 2009; Camprubi-Robles et al., 2009). In addition, excess TRPV1 activation has been shown to result in the activation of apoptosis-related cysteine proteases (called caspases) and cell death (Shin et al., 2003; Jin et al., 2005a; Amantini et al., 2007; Czaja et al., 2008).

In the present study, we show that Sox10, a transcription factor that is relevant to the development of neural crest-derived cells (Britsch et al., 2001), is a specific marker of SGCs in the adult TG and that antioxidant enzymes exhibit differential cellular localization in TG neurons and SGCs. Moreover, our cell-based studies demonstrate that excess TRPV1 activation is toxic to TRPV1-positive TG neurons because of ROS production and caspase-3 activation.

EXPERIMENTAL PROCEDURES

Animals

The *Sox10-Venus* bacterial artificial chromosome (BAC) transgenic mouse is described elsewhere (Shibata et al., 2010). Sox10 is a marker protein that is closely related to neural crest-lineage cells (Britsch et al., 2001). In the transgenic mouse, the fluorescent protein, Venus (Nagai et al., 2002), is expressed under the control of the *Sox10* promoter. As such, the generation of this transgenic mouse rendered the identification of Sox10-expressing cells feasible without immunostaining.

Male *Sox10-Venus* transgenic mice ($n = 8$; body weight, 20–25 g) were used for immunohistochemistry. Newborn rats ($n = 25$, postnatal day 2–3) were used for the preparation of primary TG cultures. All animal procedures were approved by the Laboratory Animal Care and Use Committee of our institution and were performed in accordance with the guidelines for the Care and Use of Laboratory Animals of the Keio University School of Medicine (No. 08076). All surgeries and animal care were undertaken with the utmost caution to minimize the suffering of the animals.

Immunohistochemistry

Under deep anesthesia by excess pentobarbital sodium (Somnopentyl, Schering-Plough Animal Health Corp., Summit, NJ, USA), the animals were transcardially perfused with 4% paraformaldehyde in 0.1 M phosphate buffer, pH 7.0. Immediately after the perfusion fixation, TG were dissected out and immersed in the same fixative for 4 h at 4 °C and were then kept in 0.01 M phosphate-buffered saline (PBS) solution containing 20% sucrose (w/v) for 12 h for cryoprotection. Subsequently, the TGs were embedded in Tissue TEK (Sakura Finetek, Torrance, CA, USA) and were frozen in liquid nitrogen. Serial sections of 8-μm thickness were prepared on a cryostat (Reichert-Jung Cryocut 1800; Leica Microsystems, Mannheim, Germany) in the horizontal plane along the long axis. Every 15th section was thaw-mounted on MAS-GP micro slide glass (Matsunami, Osaka, Japan) and air-dried overnight at room temperature.

The sections were pre-incubated with 10% normal donkey serum/0.1 M phosphate buffer for 30 min for blocking. They were incubated with specific primary antibodies for 48 h at room temperature. After they were washed with 0.01 M PBS, the sections were incubated with species-specific fluorophore-labeled secondary antibodies for 2 h at room temperature. After rinsing with 0.01 M PBS, the sections were coverslipped in mounting medium (buffered glycerol: pH 8.6). The primary antibodies and dilutions used in the procedure were as follows: anti-glutamate/aspartate transporter (GLAST) polyclonal antibody (raised in guinea pig; code, AB1782; Millipore, Billerica, MA, USA; 1:200) (Benediktsson et al., 2012), anti-glutamine synthase monoclonal antibody (raised in mouse; code, MAB302; Millipore; 1:500) (Marin-Valencia et al., 2012), anti-glutathione S-transferase-pi (GST-π) polyclonal antibody (raised in rabbit; code, 311; Medical & Biological Laboratories Co., Ltd., Nagoya, Japan; 1:200), anti-tubulin, βIII isoform (raised in mouse; code MAB1637; Millipore), anti-catalase polyclonal antibody (raised in rabbit; code, ab52477; Abcam, Cambridge, MA, USA; 1:200), anti-Trx2 polyclonal antibody (raised in rabbit; sc-50336; Santa Cruz Biotechnology, Santa Cruz, CA, USA; 1:50) (McCommis et al., 2011), anti-SOD1 (Cu/Zn Enzyme) polyclonal antibody (raised in sheep; code, 574597; Calbiochem, Darmstadt, Germany; 1:200), anti-SOD2 (Mn Enzyme) polyclonal antibody (raised in sheep; code, 574596; Calbiochem, 1:200), and anti-GPx1 polyclonal antibody (raised in goat; code, AF3798; R&D

Systems, Minneapolis, MN, USA, 1:100). Then, 8-hydroxy-2′-deoxyguanosine (8-OHdG) immunolabeling was accomplished using the anti-8-OHdG monoclonal antibody (raised in mouse; code, MOG-020P; Japan institute for the Control of Aging, Tokyo, Japan; 1:200) (Toyokuni et al., 1997), with the aid of a staining kit (MOM; Vector Laboratories, Burlingame, CA, USA), the latter of which was specifically designed to localize mouse primary antibodies in mouse tissues and was used according to the manufacturer's instructions. The species-specific secondary antibodies were raised in donkeys and were conjugated to Cy3, Dylight 649, or Alexa Fluor 647; all of them were obtained from Jackson Immunoresearch Laboratories (West Grove, PA, USA). The immunolabeled specimens were examined under a Leica TCS-SP5 confocal laser scanning microscopy (Leica Microsystems). In order to quantify SOD1 and SOD2 immunoreactivity, we counted SOD1- and SOD2-positive cells in randomly selected 300 neurons or SGCs. For the determination of GST-π-positive TG neurons, we measured neuronal soma diameters using image analysis software (Keyence, Osaka, Japan). The proportion of GST-π-positive cells in total TG neurons (n = 47) by diameter size was evaluated.

Behavioral testing for assessment of head withdrawal responses

A group of male Sprague–Dawley (SD) rats (n = 6) was intraperitoneally injected with 4-hydroxy-2,2,6,6-four methys piperidine (TEMPOL) (Sigma, St. Louis, MO) dissolved in saline (60 mg/ml, 300 mg/kg). Another set of male SD rats (n = 6) was intraperitoneally injected with the same volume of saline (Schwartz et al., 2008). After 10 min, mechanical sensitivity of the whisker pad was evaluated by the amount of positive head withdrawals in response to von Frey stimuli. A von Frey monofilament (3.5 g = 34.3 mN) was applied perpendicular to the stimulation site with sufficient force to bend the filament for 1 s and then slowly removed. In each session of trials, von Frey stimulation was applied 10 times, and the number of head withdrawals was counted. To assess the role of ROS in the induction and maintenance of capsaicin-induced facial hyperalgesia, we applied a piece of square filter paper soaked with capsaicin (10 mM in DMSO) (Sigma) to the left whisker pad for 30 min under light anesthesia with sodium pentobarbital (40 mg/kg, i.p.) 30 min after the pretreatment with either TEMPOL or saline (Honda et al., 2008). For reference, DMSO-soaked square filter paper was applied to the right whisker pad. After 30 min, the filter paper was removed, and the development of flare in the skin treated with capsaicin was recognized. During the procedure, body temperature was maintained at 37 °C using a rectal thermistor-controlled heating pad. Two hours after the removal of filter paper, we confirmed that anesthesia had worn off in all the rats, and mechanical sensitivity was assessed by applying a von Frey monofilament to the site of the flared skin on the side of capsaicin application and the corresponding site on the contralateral side. Subsequently, the assessment of mechanical sensitivity was repeated at 6 and 24 h after the capsaicin treatment. All the animals had been habituated to the monofilament stimulation for the last 7 days before the behavioral testing. The statistical analysis was performed using a two-way ANOVA with one repeated factor (time) and t-test for between-group difference. $p < 0.05$ was considered statistically significant.

Stable transformants expressing an enhanced GFP-full-length rat TRPV1 fusion protein

Total RNA was prepared from the TG of an adult male Sprague–Dawley rat using TRIZOL LS Reagent (Invitrogen, Carlsbad, CA, USA). From an aliquot of 1 μg of total RNA, cDNA was synthesized employing the SuperScript III RT First-Strand Synthesis System (Invitrogen) according to the manufacturer's instructions. Full-length *TRPV1* cDNA was amplified by PCR using a set of sequence-specific primers (forward; 5′-ggaattctg gaacaacgggctagcttagac-3′, reverse; 5′-ggggtaccttatttct cccctgggaccat-3′). The full-length *TRPV1* cDNA PCR fragment was subcloned into the pEGPP-C3 plasmid (Clontech, Mountain View, CA, USA), which had a G418 resistance gene expression cassette, and the resultant vector was designed to express an enhanced green fluorescent protein (EGFP)-full length rat TRPV1 fusion protein in mammalian cells. The integrity of the vector was confirmed by DNA sequencing. The vector was transfected into the rat pheochromocytoma-derived cell line, PC12, using the Lipofectamine 2000 Transfection Reagent. PC12 cells were grown in Dulbecco's modified Eagle's medium (DMEM, Invitrogen) supplemented with 15% horse serum, 2.5% fetal bovine serum, 50 units penicillin and 50-μg streptomycin. Successfully transfected cells were identified by GFP signals under fluorescence microscopy. Stable transformants were selected by continuously adding G418 (final concentration, 700 μg/ml) to the medium and were grown until clonal colonies could be isolated.

Capsaicin treatment and Western blot analysis

Capsaicin (Sigma), the TRPV1 antagonist, capsazepine (Sigma), and the cell permeant ROS scavenger, TEMPOL (Sigma), were dissolved in dimethylsulfoxide (DMSO) at 100 mM, 50 mM, and 1 M, respectively. PC12 cells were then divided into several groups. The control cell group was treated with vehicle (0.1% DMSO) for 30 min, and the capsaicin-treated cell groups were exposed to capsaicin at concentrations of 1, 10 or 100 μM for 30 min. In separate groups, cells were treated with 100 μM capsaicin for 30 min, which was accompanied by capsazepine (50 μM) or the free radical scavenger, TEMPOL (0.5 M or 1 M), with treatment starting 30 min prior to and continuing throughout the capsaicin treatment. Following the pharmacological treatment, the cells were harvested, and cell lysates were prepared using Laemmli sample buffer (Biorad, Hercules, CA, USA). The samples were subjected to SDS–PAGE, and proteins were transferred

to PVDF membranes (Immobilon-P, Millipore). The membranes were incubated with primary antibodies overnight at 4 °C. After rinsing with Tris-buffered saline/0.1% Tween-20 (TBS-T), the blots were then incubated with species-specific horse radish peroxidase (HRP)-conjugated secondary antibodies for two hours at room temperature. Immunoreactive bands were visualized by the enhanced chemiluminescence reaction with Western Lightning-ECL Plus (PerkinElmer, Waltham, MA, USA), and images were captured with a CCD camera connected to the ImageQuant LAS 4000 system (Fuji Film, Tokyo, Japan). The primary antibodies and dilutions used in this study were as follows: anti-TRPV1 (TransGenic, Kumamoto, Japan, 1:1000), anti-GFP (MBL, Nagoya, Japan, 1:1000), anti-phospho-c-Jun N-terminal kinase (phospho-JNK) (Cell Signaling Technology, Danvers, MA, 1:1000), anti-total c-Jun N-terminal kinase (total JNK) (Santa Cruz Biotechnology, Santa Cruz, CA, 1:1000), anti-active caspase-3 (Cell Signaling, 1:1000), anti-α-tubulin (Sigma, 1:100,000) and anti-GAPDH (Cell Signaling, 1:1000). All of the secondary antibodies were purchased from Jackson ImmunoResearch (West Grove, PA, USA). Densitometric analysis of immunoreactive bands for phospho-JNK and total JNK was performed using Multigauge software ver. 3.3 (Fuji Film, Tokyo, Japan). The ratio of phospho-JNK to total JNK (phospho-JNK/total JNK) was calculated in each sample. Data shown represent the mean ± SD. The fold change of the ratio of phospho-JNK/total JNK from the corresponding ratio in the vehicle sample was evaluated by employing a one-way analysis of variance (ANOVA) and Bonferroni's post hoc test. We used IBM SPSS, ver. 19 (Chicago, IL) for statistical analysis. Statistical significance was set at $p < 0.05$.

Reverse transcription-polymerase chain reaction for TRPV1 and GAPDH

For a rat TG tissue sample, RNA extraction and reverse transcription-polymerase chain reaction (RT-PCR) for *TRPV1* were performed as described in the Section 4. For PC12 cells, approximately 1×10^7 cells grown on a culture dish were collected as a pellet by centrifugation. RNA extraction and RT-PCR for *TRPV1* were conducted as described above. The primers for the TRPV1 transcript were designed to amplify both endogenous and recombinant rat full-length *TRPV1* cDNA. For the internal control of the RT-PCR, we amplified a rat *GAPDH* cDNA fragment using a set of sequence-specific primers: forward, 5′-atggtgaaggtcggt gtgaacgga-3′, and reverse, 5′-acgatgccaaagttgtcatggat g-3′. PCR products were electrophoresed in 1% agarose gels.

TRPV1-positive neuron survival assay using rat primary TG cultures

Rat primary TG cultures were prepared from neonatal Sprague–Dawley rats (2–3 days old). Briefly, after dissection, TG tissue samples were minced in ice-cold HBSS (Hank's balanced saline solution; Invitrogen). After centrifugation, the pellet was resuspended in Leibovitz L15 (Invitrogen) containing 250 U/ml collagenase (Worthington, Lakewood, NJ, USA), 1 U/ml elastase (Worthington), and 5 U/ml papain (Worthington), and the suspension was incubated for 1.5 h at 37 °C. Cells were grown in DMEM/F12 (Invitrogen) supplemented with 10% FBS, 50 ng/ml NGF (Sigma), and 1% penicillin/streptomycin (Invitrogen). At Day 2 of culture, the cells were treated with different concentrations (100 nM, 1 μM and 10 μM) of capsaicin for 30 min. In parallel, for 10 μM capsaicin, treatment with either TEMPOL or the pancapsase inhibitor, zVAD, 30 min prior to and continuing capsaicin treatment was performed. After the pharmacological interventions, the cultured cells were fixed with 2% paraformaldehyde/PBS and immunostained with anti-TRPV1 antibody (raised in a rabbit; code KM 018; TransGenic, Kumamoto, Japan; 1:200). Immunofluorescent images were randomly captured using a fluorescence microscope. The number of TRPV1-positive neurons in each treatment group was counted and expressed as the mean ± SD% of that in the vehicle-treated control culture. Statistical analysis was performed by a one-way ANOVA and Bonferroni's post hoc test using IBM SPSS, ver. 19. Statistical significance was set at $p < 0.05$.

RESULTS

Sox10-Venus expression in TG

We examined the distribution of Venus expression in TG of adult *Sox10-Venus* BAC transgenic mice. In the TG cell architecture, the Venus-derived fluorescence signal was localized exclusively to small cells that ensheathed TG neurons. Meanwhile, TG neurons were devoid of Venus signals. Judging from the morphology and distribution of the Venus-positive cells, we surmised that they were SGCs. To confirm this observation, we conducted immunostaining for two established markers for SGCs in TG: glutamine synthase and GLAST. There was clear co-localization of Venus with both markers (Fig. 1), indicating that Sox10 expression is restricted to SGCs in adult mouse TG. There was no difference in the distribution pattern of glutamine synthase in TG between the wild-type and *Sox10-Venus* BAC transgenic mouse (Fig. 1E).

Expression of proteins related to reactive oxygen species catabolism in TG

As described above, the *Sox10-Venus* BAC transgenic mouse proved to be a useful tool for identifying SGCs in TG. We performed an immunohistochemical screening for protein expression in SGCs by employing this transgenic mouse, and we found that immunoreactivity for the oxidative stress marker, 8-OHdG, was prominent in SGCs (Fig. 2). Hence, this observation prompted us to study the localization of antioxidant enzymes in TG. Because 8-OHdG immunoreactivity was not observed in neurons, we reasoned that SGCs were subjected to more oxidative stress compared to neurons. We then

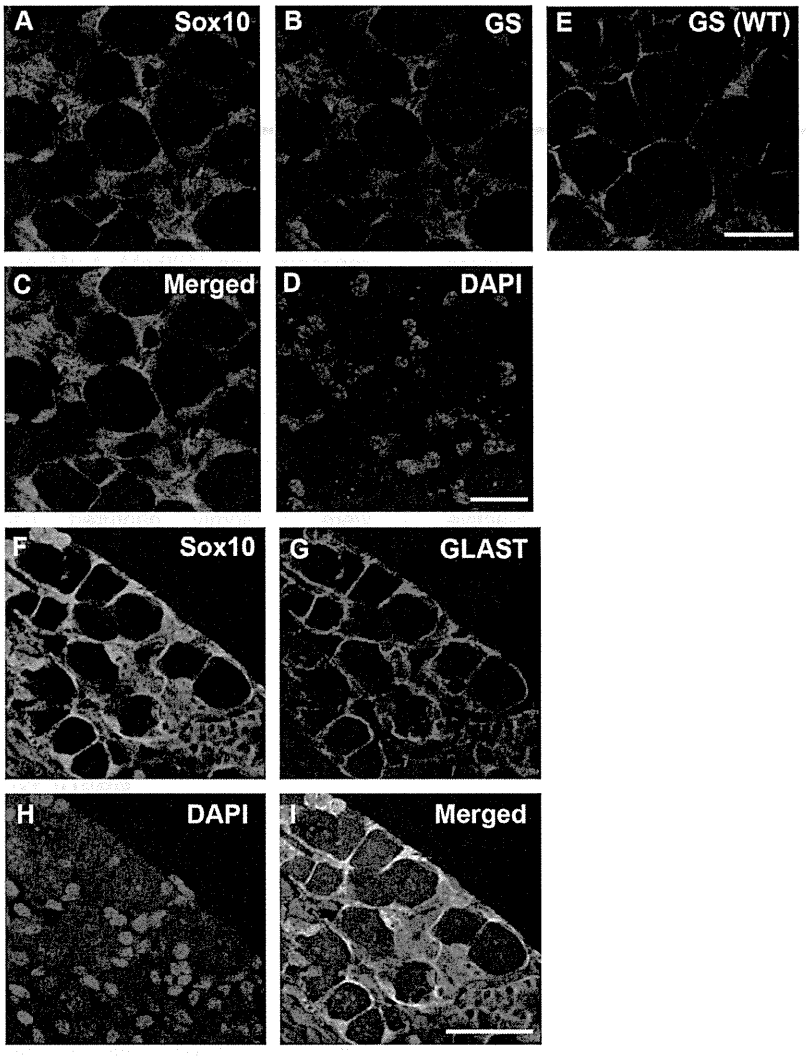

Fig. 1. Co-localization of the Venus signal with the SGC markers, glutamine synthase and GLAST, in *Sox10-Venus* BAC transgenic mouse TG. (A) Sox10 (Venus), (B) glutamine synthase, (C) merged image, (D) DAPI (nuclear staining), Scale bars = 20 μm, (E) glutamine synthase in wild-type mouse TG, Scale bar = 20 μm, (F) Sox10, (G) GLAST, (H) DAPI, (I) merged image, Scale bar = 25 μm.

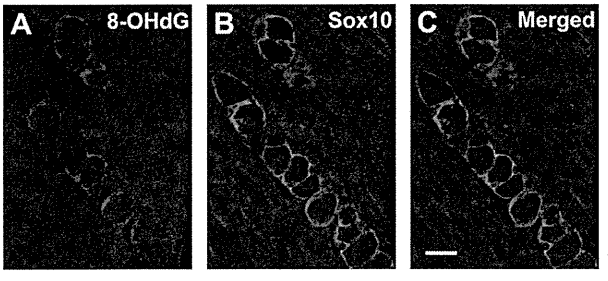

Fig. 2. The oxidative marker, 8-OHdG, was recognized in Sox10-expressing SGCs in TG. (A) 8-OHdG, (B) Sox10 (Venus), (C) merged image. Scale bars = 25 μm.

conducted single immunohistochemical labeling experiments using antibodies against SOD1 and 2 (Fig. 3), GPx1 (Fig. 4A–C), catalase (Fig. 4D–F), Trx2 (Fig. 4G–I) and GST-π (Fig. 5). SOD 1 and 2 displayed distinct cellular localizations, such that SOD1 was present in both neurons and SGCs, whereas SOD2 was localized exclusively in neurons (Fig. 3). Quantitatively, SOD1 immunoreactivity was recognized in 96.3% of TG neurons (n = 300) and 41.0% of SGCs (n = 300), whereas SOD2 immunoreactivity was identified in 94% of TG neurons (n = 300). GPx1 was identified only in neurons (Fig. 4A–C). In contrast, catalase expression was restricted to SGCs (Fig. 4D–F). Meanwhile, Trx 2 was present in both neurons and SGCs (Fig. 4G–I). Immunoreactivity for GST-π was discernible primarily in SGCs (Fig. 5A–C, arrows). However, weak immunoreactivity was also present in a subset of small- to medium-sized (diameter < 35 μm) neurons (Fig. 5A–C, arrowheads; Table 1 for quantification), which were positive for the neuronal marker, βIII-tubulin (Fig. 5D–H).

ROS is involved in capsaicin-induced mechanical hyperalgesia in the trigeminal territory

Mechanical sensitivity of the rat whisker pad was assessed by the amount of positive head withdrawals in

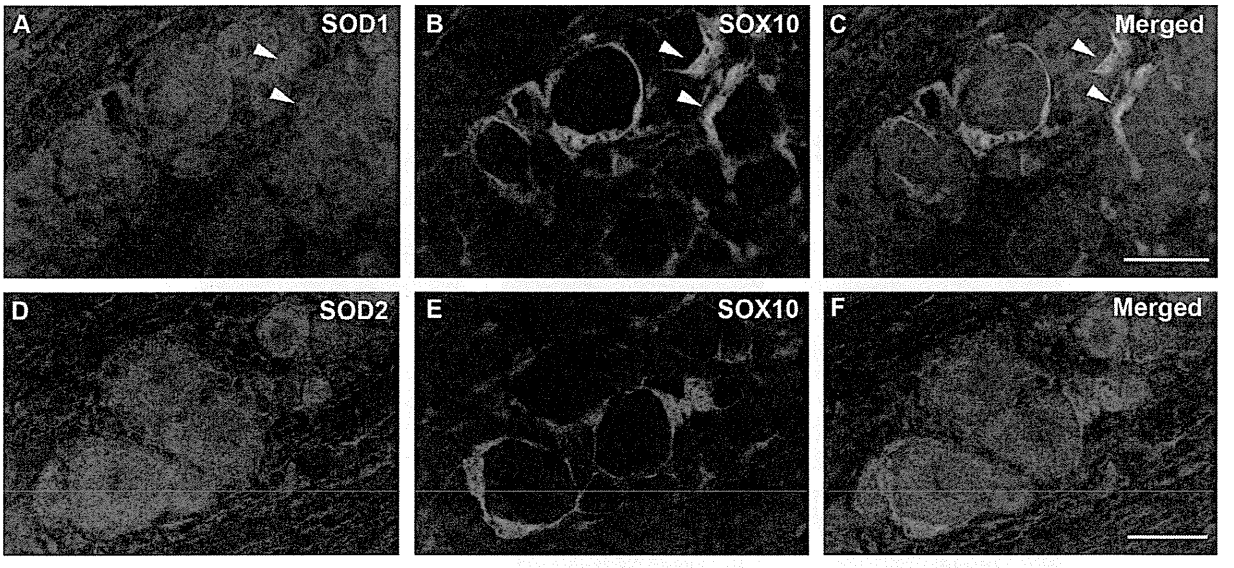

Fig. 3. Localization of SOD1 and 2 in TG. (A) SOD1 (left), Sox10 (middle), merged image (right). Arrowheads indicate SOD1-positive SGCs. (B) SOD2 (left), Sox10 (middle), merged image (right). Scale bars = 25 μm. The images were obtained from a TG section of the *Sox10-Venus* BAC transgenic mouse.

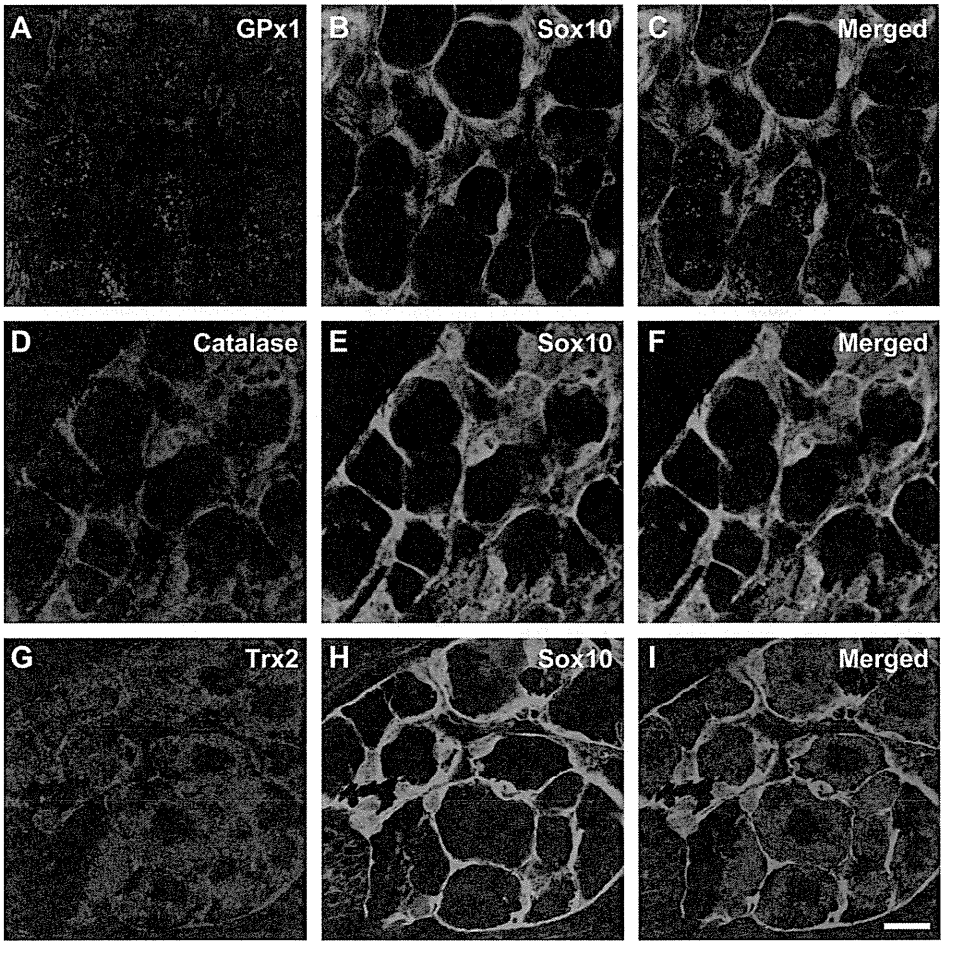

Fig. 4. Cellular localization of GPx1, catalase and Trx2 in TG. (A) GPx1, (B) Sox10, (C) merged image, (D) catalase, (E) Sox10, (F) merged image, (G) Trx2, (H) Sox10, (I) merged image. Scale bars = 25 μm. The images were obtained from a TG section of the Sox10-Venus transgenic mouse.

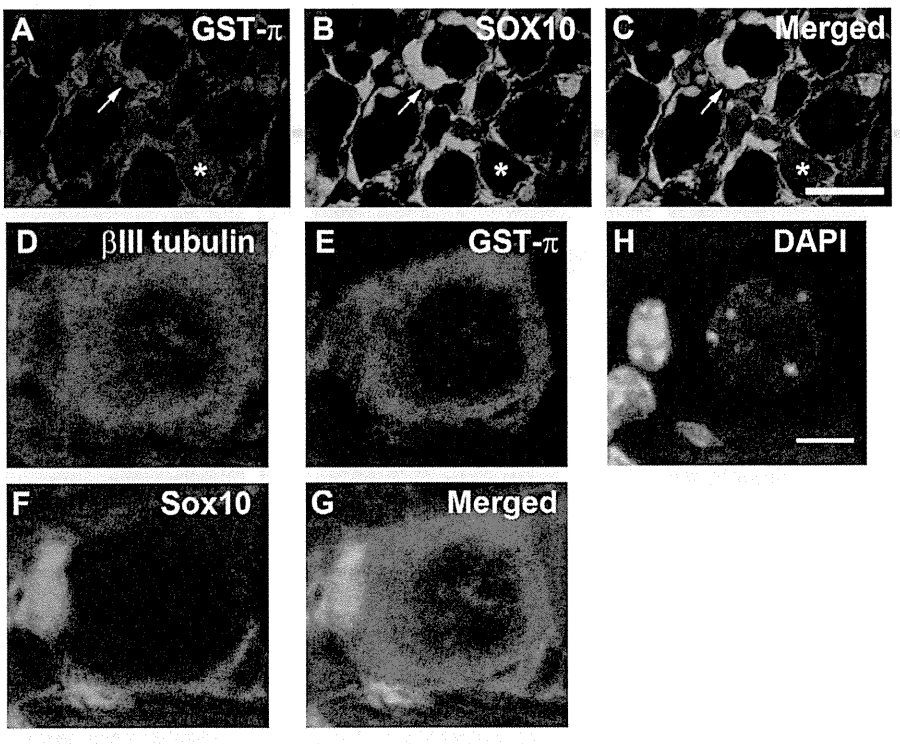

Fig. 5. Localization of GST-π in TG. (A) GST-π, (B) Sox10, (C) merged image. Immunoreactivity for GST-π is recognized in Sox10-positive SGCs (arrows). Small- to middle-sized neurons exhibit weak immunoreactivity for GST-π (asterisk). Scale bars = 25 μm. (D) βIII tubulin, (E) GST-π, (F) Sox10, (G) merged image, (H) DAPI. Scale bar = 15 μm. The two sets of images (A–C and D–H) were obtained from two distinct TG sections of the Sox10-Venus transgenic mouse.

Table 1. Proportion of GST-π-positive cells in TG neurons by diameter size. A total of 47 TG neurons were analyzed

Diameter (μm)	Number	GST-π-positive neurons (%)
10–15	5	60.0
16–20	12	33.3
21–25	13	69.2
26–30	9	33.3
31–35	4	25.0
36–40	3	0
41–45	1	0

response to von Frey monofilament stimulation. Topical capsaicin application to the whisker pad induced mechanical hyperalgesia, which was evidenced by increased frequency of head withdrawals. The mechanical hyperalgesia was most prominent at 2 h after capsaicin treatment (1.8 ± 1.8 at pretreatment to 5.7 ± 4.1 at 2 h, $p = 0.026$, paired t-test, $n = 6$ in each group, Fig. 6). With treatment with TEMPOL, a well-established ROS scavenger, the mechanical hyperalgesia was attenuated (5.7 ± 4.1 in the TEMPOL-treated group vs. 1.6 ± 2.4 in the saline-treated group, $p = 0.044$, unpaired t-test, $n = 6$ in each group).

Capsaicin treatment induces ROS-mediated caspase-3 activation in high TRPV1-expressing PC12 cells

Several PC12 cell lines that stably expressed an EGFP-full-length TRPV1 fusion protein (EGFP-flTRPV1) were obtained. In most of these cell lines, Western blot analysis identified a distinct band that was immunoreactive for both TRPV1 and GFP at the molecular weight of 115 kDa, which was consistent with the expected molecular weight of the EGFP-flTRPV1 fusion protein (Fig. 7A, lanes 2 and 3). Incidentally, we obtained a PC12 cell line that failed to express the fusion protein in spite of acquiring resistance to G418 after the transfection procedure (Fig. 7A, lane 1). This cell line was designated as the EGFP-flTRPV1-null cell line. In this cell line, there was no discernible endogenous TRPV1 protein expression by Western blot. Because RT-PCR analysis revealed the presence of *TRPV1* mRNA, it seemed likely that there was translational down-regulation of the *TRPV1* transcript (Fig. 7B, lane 2). JNK phosphorylation is known to be an important step in the signal transduction pathway activated by ROS exposure (McCubrey et al., 2006). Hence, we assayed JNK phosphorylation in cells exposed to capsaicin treatment. There was a robust increase in JNK phosphorylation in the high EGFP-flTRPV1-expressing cell line after the capsaicin treatment in a dose-dependent manner (for p54, 26.81 ± 0.61-fold at 10 μM and 52.09 ± 2.97-fold at 100 μM compared to the vehicle-treated cells, $p < 0.001$; for p46, 35.50 ± 1.07-fold at 10 μM and 64.90 ± 3.17-fold at 100 μM compared to the vehicle-treated cells, $p < 0.001$) (Fig. 8A, B). Capsaicin treatment at 100 μM beyond 30 min was found to cause JNK protein degradation (data not shown). Therefore, we reasoned that capsaicin treatment at 100 μM for 30 min was the

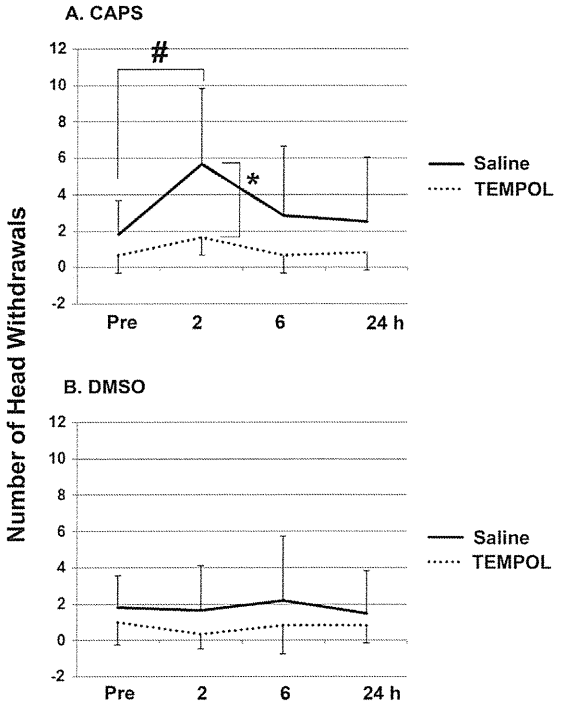

Fig. 6. Capsaicin-induced nocifensive head withdrawals. The numbers of head withdrawals in response to von Frey stimulation were counted on the capsaicin (10 mM)-treated side (A) and vehicle (DMSO)-treated side. To explore the involvement of ROS production, TEMPOL (300 mg/kg) was intraperitoneally injected 30 min before the capsaicin application in six animals (dotted lines). For controls, the same volume of saline was intraperitoneally injected in six animals (solid lines). The data are expressed as the mean ± SD. The interaction between the time course and head withdrawal numbers was assessed by a two-way ANOVA. Comparison within the same group between two time points was made by paired *t*-test. Between group comparisons were performed by unpaired *t*-test. $^{\#}p < 0.05$ vs. the pretreatment group (Pre), $^{*}p < 0.05$ between the saline- and TEMPOL-treated groups.

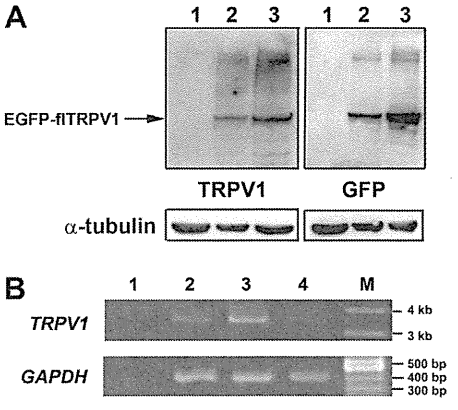

Fig. 7. Characterization of EGFP-flTRPV1-expressing PC12 cell lines by Western blot and RT-PCR. (A) Western blot data for TRPV1 (left) and GFP (right) expression. Lane 1: EGFP-flTRPV1-null cell line, Lane 2: moderate EGFP-flTRPV1-expressing cell line, Lane 3: high EGFP-flTRPV1-expressing cell line. The arrow indicates immunoreactive bands that represent the EGFP-flTRPV1 fusion protein. (B) RT-PCR for rat *TRPV1* and *GAPDH* transcripts. Lane 1: negative control, Lane 2: EGFP-flTRPV1-null cell line, Lane 3: recombinant rat full-length *TRPV1* cDNA. Lane 4: rat TG. M, markers.

optimal condition for examining capsaicin-induced JNK phosphorylation in our experimental conditions. JNK phosphorylation was lessened by 100 μM capsazepine treatment (for p54, 55.64 ± 3.98-fold at 100 μM CAPS vs. 24.58 ± 1.78-fold at 100 μM CAPS + 100 μM capsazepine compared to the vehicle-treated cells, $p < 0.001$; for p46, 75.54 ± 11.19-fold at 100 μM CAPS vs. 20.52 ± 2.14-fold at 100 μM CAPS + 100 μM capsazepine compared to the vehicle-treated cells, $p < 0.001$) (Fig. 8C), indicating that the capsaicin-induced JNK phosphorylation was a TRPV1 ligand-dependent process. TEMPOL attenuated capsaicin-induced JNK phosphorylation in a dose-dependent manner (Fig. 8C). Meanwhile, the EGFP-flTRPV1-null cell line did not exhibit any significant alteration in JNK phosphorylation (Fig. 8A, B). Several lines of evidence show that ROS overproduction induces caspase-3-mediated cell death (Franklin, 2011). Exposure of the high EGFP-flTRPV1-expressing cell line to 100 μM capsaicin induced cell rounding and a detachment of cells from the culture dish, starting at as early as 30 min; these changes are morphological changes that are indicative of cell demise (Fig. 9A). These morphological alterations were prevented by capsazepine. Next, we examined casapse-3 activation in the high EGFP-flTRPV1-expressing cell line. Our preliminary experiments showed that 3 h of capsaicin treatment is the most appropriate time point for examining the activation of caspase-3 (data not shown). Caspase-3 activation became obvious at this time point in a dose-dependent manner (Fig. 9B). Such capsaicin-induced caspase-3 activation was abolished by TEMPOL, indicating that ROS production was implicated in this process (Fig. 9C).

Capsaicin treatment induces caspase- and ROS-mediated cell demise of TRPV1-positive TG neurons

To assess the neurotoxic effects of capsaicin on TG neurons, we applied capsaicin to primary TG cultures and measured the number of remaining TRPV1-positive TG neurons. Capsaicin induced a dose-dependent loss of TRPV1-positive neurons (Fig. 10). The capsaicin-induced neuronal loss was prevented by TEMPOL and z-VAD pretreatment.

DISCUSSION

Sox10 expression in adult TG

Sox10 is a transcriptional factor that plays a pivotal role in the development of neural crest-derived cells. In DRG, Sox10 expression is primarily recognized in neurons at embryonic day 11.5, but neurons have ceased to express Sox10 by embryonic day 15.5 (Shibata et al., 2010). However, little is known about Sox10 expression in TG, especially in adulthood. To our knowledge, the present study provides the first evidence that Sox10 is expressed exclusively in SGCs in adult TG. In addition to the previous observation that spontaneous or targeted disruption of Sox10 resulted in a loss of

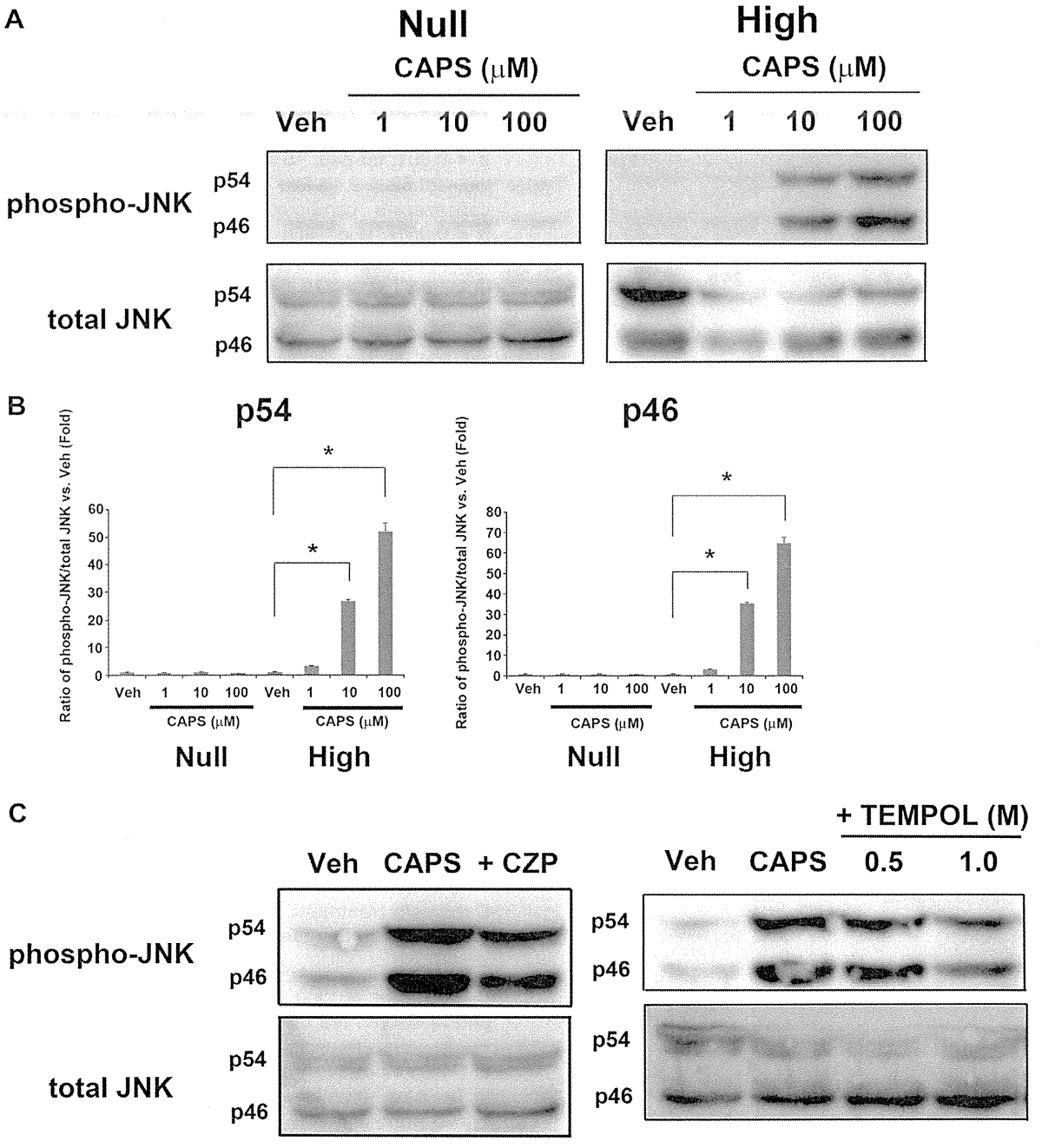

Fig. 8. Capsaicin enhances JNK phosphorylation via TRPV1 activation in the high EGFP-flTRPV1-expressing cell line. (A) Western blot data for phosphorylated (phospho-JNK) and total JNK. JNK is identified as two distinct bands that represent p54 and p46. High: high EGFP-flTRPV1-expressing cell line, Null: EGFP-flTRPV1-null cell line, Veh: vehicle (0.1% DMSO), CAPS: capsaicin. The duration of capsaicin exposure was 30 min. (B) Densitometric data for phospho-JNK/total JNK (separately for p54 and p46) ratio against the vehicle sample (Veh). The data are expressed as the mean ± SD ($n = 4$ in each group). $^{*}p < 0.001$, versus Veh, a one-way ANOVA, Bonferroni's post hoc test. (C) Effects of capsazepine and TEMPOL on capsaicin-induced JNK phosphorylation in high EGFP-flTRPV1-expressing cell line. Treatment with either capsazepine (50 μM) or the free radical scavenger, TEMPOL (0.5 M or 1 M), was started 30 min prior to capsaicin treatment and was continued throughout the capsaicin treatment. CAPS, capsaicin; +CZP, capsaicin + capsazepine.

Schwann cells and satellite cells in DRG (Britsch et al., 2001), our finding suggests that Sox10 is important in the development and maintenance of the SGCs in neural crest-derived ganglia.

Cellular distribution of antioxidant enzymes in TG

Our immunohistochemical analysis revealed that antioxidant enzymes are differentially distributed in TG. Both SOD1 and 2 are localized in neurons, whereas

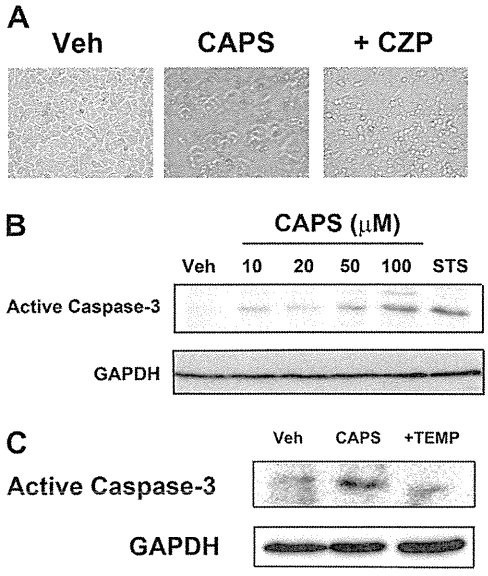

Fig. 9. Capsaicin treatment leads to caspase-3 activation via ROS production in the high EGFP-flTRPV1-expressing cell line. (A) Micrographs showing cell morphology treated with the vehicle (0.1% DMSO, Veh), capsaicin (100 μM, CAPS) or capsaicin (100 μM) + capsazepine (100 μM) (+CZP). The duration of capsaicin treatment was 30 min, with capsazepine treatment starting 30 min prior to and continuing throughout capsaicin treatment. (B) Western blot data for active (cleaved) caspase-3. Staurosporine (STS) was used as a positive control agent for activation caspase-3. The blot is representative of 3 independent studies. Veh, vehicle (0.1% DMSO); CAPS, capsaicin; STS, staurosporine (2.5 μM). The duration of staurosporine treatment was 16 h. (C) Effect of TEMPOL pretreatment on capsaicin-induced casapse-3 activation. The duration of capsaicin treatment was 3 h, and TEMPOL administration was started 30 min prior to capsaicin treatment, and was continued throughout capsaicin treatment. Veh, vehicle (0.1% DMSO); CAPS, capsaicin (100 μM); +TEMP, capsaicin (100 μM) + TEMPOL (1 M). The blot is representative of three independent studies.

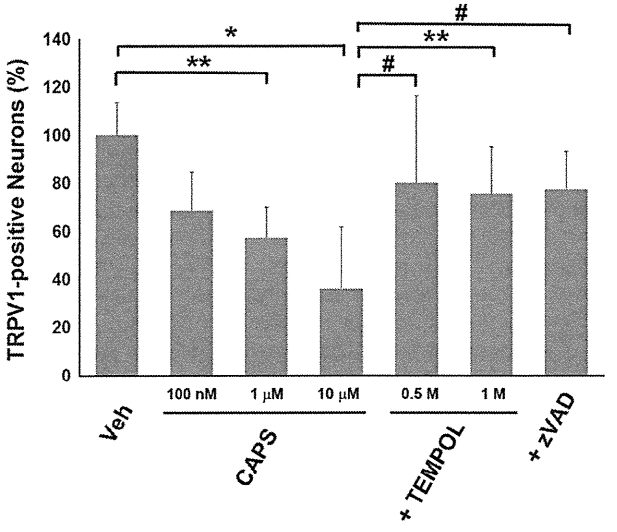

Fig. 10. Capsaicin-induced cell demise of TRPV1-positive TG neurons. The number of TRPV1-positive TG neurons in each group was shown as mean ± SD% of the vehicle-treated cells. $^{*}p < 0.001$, $^{**}p < 0.01$, $^{\#}p < 0.05$, a one-way ANOVA, Bonferroni's post hoc test.

SGCs are provided with SOD1 alone. The enzymes with H_2O_2-decomposing activity, GPx1 and catalase, displayed differential cellular localization patterns, such that GPx1 and catalase are exclusively distributed in neurons and SGCs, respectively. The predominant localization of GPx1 in neurons over glial cells has also been reported in human brain tissue (Power and Blumbergs, 2009). Recently, the Trx/peroxiredoxin system has been recognized as another important peroxide-removing system in a variety of cellular systems, including neural cells (Patenaude et al., 2005; Bell and Hardingham, 2011). Trx2 is a mitochondrial enzyme that contains two redox-active cysteine residues (Cys-Gly-Pro-Cys) within its catalytic site. These cysteines exist in their -SH form in the reduced state and form an intramolecular disulfide bond in the oxidized state. Trx2 activates the peroxide scavengers, peroxiredoxins, by regulating their redox state (Bell and Hardingham, 2011). The present study showed that Trx2 is localized to both neurons and SGCs. Superoxide anion ($O_2^{\cdot -}$) reacts with nitric oxide to form peroxynitrite, a molecule that is exquisitely detrimental to cells. SOD1 and 2 protect cells from the toxicity of the superoxide anion by converting it to H_2O_2. H_2O_2 per se is not readily damaging to biological molecules in physiological micromolar concentrations. However, unless it is efficiently eliminated from tissue, hydroxyl radical ($^{\cdot}OH$) formation by the iron-catalyzed Fenton reaction follows. Hydroxyl radical can cause lipid peroxidation, which oxidizes amino acid side chains in proteins and induces aberrant DNA modifications, thus causing cell damage (Dringen et al., 2005). To maintain the integrity of H_2O_2-removing systems, it is therefore imperative to bypass such oxidative damage, especially in neural tissue with high oxygen demands. Because the cell viability of neurons must be maintained over a lifetime, it appears reasonable that TG neurons are endowed with more thorough antioxidant systems than SGCs. The relative importance of GPx, catalase and peroxiredoxins in neural cells has been a matter of debate (Mitozo et al., 2011). Generally, GPx1 is considered to be the primary peroxide-degrading enzyme, and this view has been corroborated by several *in vivo* experiments. The *GPx1* knockout mouse brain exhibited increased apoptosis following ischemia/reperfusion injury and cold injury (Crack et al., 2001; Flentjar et al., 2002) and exacerbated dopaminergic cell damage induced by *N*-methyl-4-phenyl-1,2,3,6-tetrahydropyridine (MPTP) (Zhang et al., 2000) compared to the wild-type mouse brain. The contribution of the Trx/peroxiredoxin system to the clearance of H_2O_2 in neural tissue is poorly understood. The inactivation of peroxiredoxins by the Trx reductase inhibitor, auranofin, caused DNA damage in astrocytoma-derived C6 cells but not in N2a neuroblastoma cells or in hippocampal tissue slices (Mitozo et al., 2011). Catalase deficiency was found to compromise the NAD-linked electron transfer activities and energy coupling capacities of brain mitochondria (Ho et al., 2004). Moreover, pharmacological catalase inhibition retarded H_2O_2 decomposition in hippocampal slices and N2a neuroblastoma cells (Mitozo et al.,